Received: 20 July 2017 | Revised: 7 September 2017 | Accepted: 11 September 2017

DOI: 10.1002/glia.23236

GLIA
WILEY

RESEARCH ARTICLE

Ulk4 deficiency leads to hypomyelination in mice

Min Liu[1] | Ping Xu[2] | Zhenlong Guan[3] | Xiaohong Qian[2] | Peter Dockery[4] | Una Fitzgerald[5] | Timothy O'Brien[1] | Sanbing Shen[1]

[1]Regenerative Medicine Institute, School of Medicine, National University of Ireland (NUI) Galway, Galway, Ireland

[2]State Key Laboratory of Proteomics, National Center for Protein Sciences, Beijing Proteome Research Center, National Engineering Research Center for Protein Drugs, Beijing Institute of Radiation Medicine, Beijing, 102206, China

[3]Department of Physiology, College of Life Science, Hebei Normal University, Shijiazhuang, China

[4]Anatomy, School of Medicine, National University of Ireland (NUI) Galway, Galway, Ireland

[5]National Centre for Biomedical Engineering Science, Galway Neuroscience Centre, National University of Ireland (NUI) Galway, Galway, Ireland

Correspondence
Sanbing Shen, Regenerative Medicine Institute, School of Medicine, National University of Ireland (NUI) Galway, Galway, Ireland.
E-mail: sanbing.shen@nuigalway.ie

Abstract

Brain nerve fibers are insulated by myelin which is produced by oligodendrocytes. Defects in myelination are increasingly recognized as a common pathology underlying neuropsychiatric and neurodevelopmental disorders, which are associated with deletions of the *Unc-51-like kinase 4* (*ULK4*) gene. Key transcription factors have been identified for oligodendrogenesis, but little is known about their associated regulators. Here we report that Ulk4 acts as a key regulator of myelination. Myelination is reduced by half in the *Ulk4*$^{tm1a/tm1a}$ hypomorph brain, whereas expression of axonal marker genes *Tubb3*, *Nefh*, *Nefl* and *Nefm* remains unaltered. Transcriptome analyses reveal that 8 (*Gfap*, *Mbp*, *Mobp*, *Plp1*, *Slc1a2*, *Ttr*, *Cnp*, *Scd2*) of the 10 most significantly altered genes in the *Ulk4*$^{tm1a/tm1a}$ brain are myelination-related. Ulk4 is co-expressed in Olig2^{+} (pan-oligodendrocyte marker) and CC1^{+} (mature myelinated oligodendrocyte marker) cells during postnatal development. Major oligodendrogeneic transcription factors, including *Olig2*, *Olig1*, *Myrf*, *Sox10*, *Sox8*, *Sox6*, *Sox17*, *Nkx2-2*, *Nkx6-2* and *Carhsp1*, are significantly downregulated in the mutants. *mRNA* transcripts enriched in oligodendrocyte progenitor cells (OPCs), the newly formed oligodendrocytes (NFOs) and myelinating oligodendrocytes (MOs), are significantly attenuated. Expression of stage-specific oligodendrocyte factors including *Cspg4*, *Sox17*, *Nfasc*, *Enpp6*, *Sirt2*, *Cnp*, *Plp1*, *Mbp*, *Ugt8*, *Mag* and *Mog* are markedly decreased. Indirect effects of axon caliber and neuroinflammation may also contribute to the hypomyelination, as *Ulk4* mutants display smaller axons and increased neuroinflammation. This is the first evidence demonstrating that ULK4 is a crucial regulator of myelination, and ULK4 may therefore become a novel therapeutic target for hypomyelination diseases.

KEYWORDS

hypomyelination, knockout mice, oligodendrogenesis, Ulk4, white matter integrity

1 | INTRODUCTION

The *Unc-51 Like Kinase 4* (*ULK4*) gene is proposed as a rare susceptibility factor of brain disorders by copy number variation studies, as hemizygous deletions of the *ULK4* gene are identified in ~1/1000 patients with schizophrenia, autism, bipolar disorder, developmental delay, language delay, or intellectual disability (Lang et al., 2014; Liu, Guan, Shen, Flinter, et al., 2016). The full length ULK4 is a 142 kDa protein containing a Ser/Thr kinase domain (predicted to be inactive) at the N-terminus and armadillo repeat sequence (ARM)-like regions in the middle/C-terminus. Although we have some knowledge about other members of the ULK family (ULK1–3 and STK36) in terms of mechanism of action, this is not the case for ULK4, and direct effects of ULK4 have not been specified.

Of major interest here is the finding that white matter abnormality is an element of the underlying pathology in these disorders. The corpus callosum (CC) is the major nerve fiber tract of axons coordinating the left and right brain activity. In human patients, agenesis of CC is common in schizophrenia (Chinnasamy, Rudd, & Velakoulis, 2006; Motomura, Satani, & Inaba, 2002; Paul et al., 2007; Swayze et al., 1997; Wolf, Hose, Frasch, Walter, & Vasic, 2008), bipolar disorder (Caetano et al., 2008), autism (Innocenti, Ansermet, & Parnas, 2003; Wolff et al., 2015) and attention-deficit disorder (Hynd et al., 1991). In animals, disruption of CC development is also reported in an idiopathic autism model of BTBR mice which exhibit selective impairment in long-range intra-hemispheric connectivity (Sforazzini et al., 2016), as well as in the *Zic2*$^{kd/+}$ and *Disc1* transgenic mouse models of schizophrenia (Hatayama et al., 2011; Shen et al., 2008) where thinned CC and cerebral cortex has been observed.

ULK4 deficiency disrupts white matter integrity (Lang et al., 2014). White matter defects are also common in congenital syndromes of ciliopathies (Bernard et al., 2012; Laclef et al., 2015) and we have recently demonstrated that Ulk4 regulates cilia development and cerebrospinal fluid (CSF) flow, as *Ulk4*$^{tm1a/tm1a}$ mutants develop congenital hydrocephalus (Liu, Guan, Shen, Lalor, et al., 2016). Other hydrocephalus models associated with overexpression of a G-protein coupled receptor (Lang et al., 2006) or mutations in *L1CAM* gene (Demyanenko, Tsai, & Maness, 1999) also display partial agenesis of CC.

White matter is myelinated by oligodendrocytes, which are differentiated from postnatal NSCs, and NSCs are reduced in *Ulk4* $^{tm1a/tm1a}$ hypomorph mice (Liu, Guan, Shen, Flinter, et al., 2016). Oligodendrocytes synthesize myelin, extend processes to contact multiple neighboring axons and enwrap short axonal segments (Baumann & Pham-Dinh, 2001). Myelinogenesis occurs predominantly in the first three postnatal weeks in rodents (Fields 2008; From et al., 2014), and in the first 2 years in children, which coincides with the diagnostic age for many neurodevelopmental disorders. Hypomyelination is common in both neurodegenerative and neurodevelopmental disorders. The advanced MRI-related techniques permits visualization of reduced and/or absent myelin, which is characterized by a delay in the development of T2 hypointensity and often T1 hyperintensity in the white matter. Now a single largest pediatric category of undiagnosed genetic leukoencephalopathies is classified as disorders with hypomyelination of white matter (Helman et al., 2015; Schiffmann & van der Knaap, 2009; Steenweg et al., 2010). Several myelin-related genes, including *CNP*, *ERBB3*, *GSN*, *MAL*, *MAG* and *TF*, are differentially expressed in schizophrenia post-mortem brain tissue compared to unaffected controls (Jungerius et al., 2008). Mice lacking *Bcas1*, a novel myelin-associated protein interacting with F-actin and the dynein light chain, exhibited schizophrenia-like abnormal behavior, upregulated inflammation and hypomyelination (Ishimoto et al., 2017).

During oligodendrogenesis, oligodendrocyte progenitor cells (OPCs) undergo 4 sequential stages of proliferation and differentiation into pro-oligodendrocytes, immature oligodendrocytes, non-myelinating and myelinating mature oligodendrocytes (Baumann & Pham-Dinh, 2001). Understanding the intrinsic regulation of oligodendroglial development may lead to the development of therapies for hypomyelination and demyelinating diseases (Back & Rosenberg, 2014). Olig2 is a master regulator of oligodendrogenesis, and regulates expression of Olig1, Sox10, Myrf, Ascl1, Nkx2-2, Yy1, Tcf4, Id2, Id4, Hes5, Sox6 and Sox5 (Emery, 2010; Nicolay, Doucette, & Nazarali, 2007). Deficiency of Olig2 abolishes the oligodendrocyte lineage (Zhou et al., 2001; Lu et al., 2002). Environmental factors including axon sizes and neuroinflammation are also known to regulate myelination (Miron, Kuhlmann, & Antel, 2011; Nave, 2010a,b; Nave & Werner, 2014).

Protein kinases have been implicated in hypomyelination. For example, excess IL-1β can also inhibit OPC maturation via suppression of FYN/MEK/ERK phosphorylation and lead to hypomyelination in rats (Xie et al., 2016). The AKT/mTOR signaling is thought responsible for the enhanced apoptosis of the Nijmegen Breakage Syndrome-mediated oligodendrocyte deficiency (Liu, Chen, Wang, & Tong, 2014). Deletion of the PI3-kinase Vps34 leads to abnormal ErbB2-ErbB3 tyrosine kinase signalling with severe hypomyelination in peripheral nerves (Logan et al., 2017). However, it was unknown if Ulk4 plays a role in myelination. We, therefore, investigated myelination in *Ulk4*$^{tm1a/tm1a}$ mice. We discovered that *Ulk4* mutants were hypomyelinated, with a ~50% reduction of myelin and a general reduction of all myelin components. Key oligodendrogeneic factors were significantly downregulated, and so were stage-specific markers of the oligodendrocyte differentiation. Ulk4 therefore acts as an important regulator of myelination.

2 | MATERIALS AND METHODS

2.1 | *Ulk4* $^{tm1a/tm1a}$ hypomorph mice

The *Ulk4*$^{+/tm1a}$ strain was created from ES cell clone EPD0182_4_E12 on C57BL/6N strain background (Skarnes et al., 2011). The gene targeting construct was generated by the Wellcome Trust Sanger Institute. Essentially, the *FRTEn2SA- IRES-LacZ-PA-hBactP-Neo-PA-FRT-loxP* cassette was inserted into intron 6, so that the *Ulk4* transcript will be truncated after exon 6 by fusion with *En2SA-IRES-LacZ-PA*. The mutant mice were created by the Mouse Biology Program (www.mousebiology.org) at the University of California, Davis. The WT allele was detected by a 271 bp PCR product using Ulk4EndE7For (5′-TAACTTGCTGGACGGATTGCTG-3′) and Ulk4EndIn7Rev (5′-TGATCT GTAATCGCAGTGCAGG-3′, and the mutant allele by appearance of a 621 bp DNA using Ulk4KOMPKOFor (5′-GAGATGGCGCAACGCA ATTA ATG-3′, and Ulk4KOMPKORev (5′-CTGAGGAGACAATGTAACC AGC-3′) as described previously (Liu, Guan, Shen, Flinter, et al., 2016; Liu, Guan, Shen, Lalor, et al., 2016). All experimental procedures were approved by the Irish Department of Health and Children in accordance with Cruelty to Animals Act of 1876 and by the institutional Animal Care and Research Ethics Committee.

2.2 | Histology

Mice were deeply anesthetized and fixed with 4% paraformaldehyde in PBS by intra-cardiac perfusion. Brains were dissected, post-fixed in the fixative solution for 24 hours and embedded into paraffin blocks. Serial coronal sections at 10 μm were processed with a microtome (SM2000R, Leica Instruments), stained with hematoxylin-eosin and imaged under a bright filed microscope (IX41, Olympus) equipped with a camera for histological analyses.

2.3 | Transmission electron microscopy (TEM)

Lateral ventricle walls were dissected from P18 mice and fixed in 2.5% glutaraldehyde/2% paraformaldehyde/0.1 M sodium cacodylate/HCl buffer (pH7.2) overnight at 4°C. Tissues were subsequently immersed in secondary fixative solution containing 1% Osmium Tetroxide in 0.1 M Sodium Cacodylate/HCl buffer (pH 7.2) for 4 h. They were then dehydrated through 50%, 70%, 90%, 95% and 100% alcohol, placed in Propylene Oxide, and transferred to a series of mixture of resin and Propylene Oxide, (50:50, 75:25, pure resin). Finally, tissues were

transferred to flat embedding molds, clearly labeled and placed in a 65°C oven for 48 h to polymerize. After polymerization, blocks were sectioned at 100 nm, lifted onto 3 mm copper grids and stained for 30 min in 1.5% aqueous Uranyl Acetate for 10 min in Lead Citrate. Sections were dried and viewed on the Hitachi H7000 TEM. Both inner and out diameter of the axons were quantified. For oval shaped axons, the narrower dimension of diameter was measured to minimize effects o section orientation.

2.4 | Immunohistochemistry

Sections were immunostained using the following primary antibodies: rabbit anti-Ulk4 (1:500, NBP1–20229, Novus Biologicals), rat monoclonal anti-Mbp (Millipore, # MAB386, 1:500) mouse monoclonal anti-Olig2 (1:1000, Millipore), rabbit polyclonal anti-Gfap (Dako, Z0334), rabbit polyclonal anti-Iba1 (#019–19741, Wako) and anti-APC antibody (CC-1, ab16794, Abcam). Fluorescent secondary antibodies were Alexa Fluor 488 goat anti-rabbit or 555 goat anti-mouse (1:500, Cell signaling) or 488 anti-Rat (1:500, ab150157). Sections were mounted with mounting medium containing DAPI (Sigma).

2.5 | Immunoblotting

P12 mouse cortex proteins were extracted with RIPA buffer containing complete protease (Roche, #11697498001) and phosphatase inhibitors (Roche, #04906845001). Soluble proteins were quantified using Pierce™ BCA Protein Assay Kit (Thermo Scientific, #23227). Proteins lysates (8 or 10 μg) were resolved on 12% SDS–PAGE and transferred to PVDF membranes (GE Healthcare Life Science, No. 10600023). The membranes were blocked with 5% skimmed milk for 1h at RT, and incubated overnight at 4°C with primary antibodies of rabbit polyclonal anti-Sox17 (Millipore, #09–038, 1:1000), or rat monoclonal anti-Mbp (Millipore, #MAB386, 1:500) or mouse monoclonal anti-Mog (Millipore, #MAB5680, 1:1000), or rabbit monoclonal anti-Gapdh (Cell Signaling, #2118, 1:1000). They were then washed and incubated for 1.5 hours at RT with a HRP-linked secondary antibody: horse anti-mouse IgG (1:2,000; Cell Signaling, #7076s), or goat anti-rabbit IgG (1:2,000; Cell Signaling, #7074s), or goat anti-rat IgG (1:2,000; Santa Cruz, sc-2032). The immunoreactive bands were visualized on X-ray film (A PLUS, Konica Minolta) using ECL kit (Thermo Scientific, # 34078) and quantified by ImageJ.

2.6 | RNA sequencing

Three pairs of P12 *Ulk4*$^{tm1a/tm1a}$ mice and WT controls were humanely terminated, and cortical RNA extracted using RNeasy Kit (QIAGEN) according to the manufacturer's instructions. RNA (~6 μg/mouse, $n = 3$ each) was sent to BGI Co. Ltd for whole genome RNA sequencing using the Illumina HiSeq2000. 19,652 genes were identified from P12 mouse cortex, and their abundance was normalized to FPKM (Fragments Per Kilobase per Million mapped fragments). *P*-value of multiple testing, FDR (false discovery rate) and one-way ANOVA were applied. $P < 0.05$ indicates statistical significance. The Ulk4 targets were narrowed to 618 genes with FPKM >1, >20% reduction and >1.5-fold induction, which were analyzed by the STRING program to identify signaling pathways.

2.7 | Quantitative RT-PCR

Quantitative RT-PCR was carried out to validate expression of key Ulk4 targets detected by the transcriptome analyses. Single strand cDNA was synthesized from P12 cortical RNA, and triple qRT-PCR were performed for each primer pair. The primers were Olig2For (5′-TGTTGCAAGAAGGGGAGCTG-3′) and Olig2Rev (5′-TCCCAGACCCTTGGAGTGTT-3′, 159bp); PdgfrbFor (5′-CAGCCCAATGAGAGTGACAA-3′) and PdgfrbRev (5′-CTCTGCTTCAGCCAGAGGTC-3′, 249 bp); Sox17For (5′-GTGCCAGGCTTCTAGTCCAG-3′) and Sox17Rev (5′-TGTGAGTGGGCCATATTTCA-3′, 192bp); MbpFor (5′-GACACCTCGAACACCACCTC-3′) and MbpRev (5′-AGAGCGGCTGTCTCTTCCTC-3′, 88, 178, 211 bp), MogFor (5′-CCTGGTTGCCTTGATCATCT-3′) and MogRev (5′-TGGAATCTGTCCACAGCAAA-3′, 173 bp). GapdhFor (5′-CTCATGACCACAGTCCATGC-3′) and GapdhRev (5′-CACATTGGGGGTAGGAACAC-3′) were used as cDNA loading control for each qRT-PCR plate. Relative RNA abundance in the *Ulk4*$^{tm1a/tm1a}$ cortex was calculated using $2^{\Delta\Delta Ct}$, with average expression level of the corresponding gene in the WT littermates as 100%. The data were presented as mean ± SEM, $n = 3$ each, * for $p < 0.05$.

2.8 | Statistical analysis

At least three different mice per genotype from two or three independent litters were used per experiment. For histology, three-six coronal brain serial sections per mouse were analyzed. The ImageJ software package was used to quantify brain areas from comparable sections, and immunoblots. Statistical significance was evaluated by two-tailed Student's t-test, with $p < 0.05$ considered indicative of statistical significance. The numbers of animals used for quantification are indicated in Figure legends.

3 | RESULTS

3.1 | Ulk4 is expressed in oligodendrocyte lineage

Previously we showed that ULK4 deficiency reduced neurite outgrowth/branching *in vitro* and compromised the CC integrity in *Ulk4*$^{tm1a/tm1a}$ newborn mice (Lang et al., 2014). Mouse white matter is myelinated predominantly within the first 3 postnatal weeks by oligodendrogenesis (From et al., 2014). The OPCs are developed from postnatal NSCs in the SVZ and undergo proliferation, differentiation and maturation to become Mbp$^+$ myelinating oligodendrocytes. Because NSCs were markedly reduced in *Ulk4*$^{tm1a/tm1a}$ newborn mice (Liu, Guan, Shen, Flinter, et al., 2016), we first immunohistochemically stain the P0, P12 and 2-month brain sections with the pan-oligodendrocyte marker anti-Olig2 and anti-Ulk4 (Figure 1A–H), and observed complete co-staining in the P0 SVZ (Figure 1A), and in the CC of P0 (Figure 1B), P12 (Figure 1C) and 2-month (Figure 1D) mouse brain. We then carried out double staining with anti-Ulk4 and CC1 antibody (anti-APC), a marker for mature oligodendrocytes (Figure 1E/e–H/h), and detected

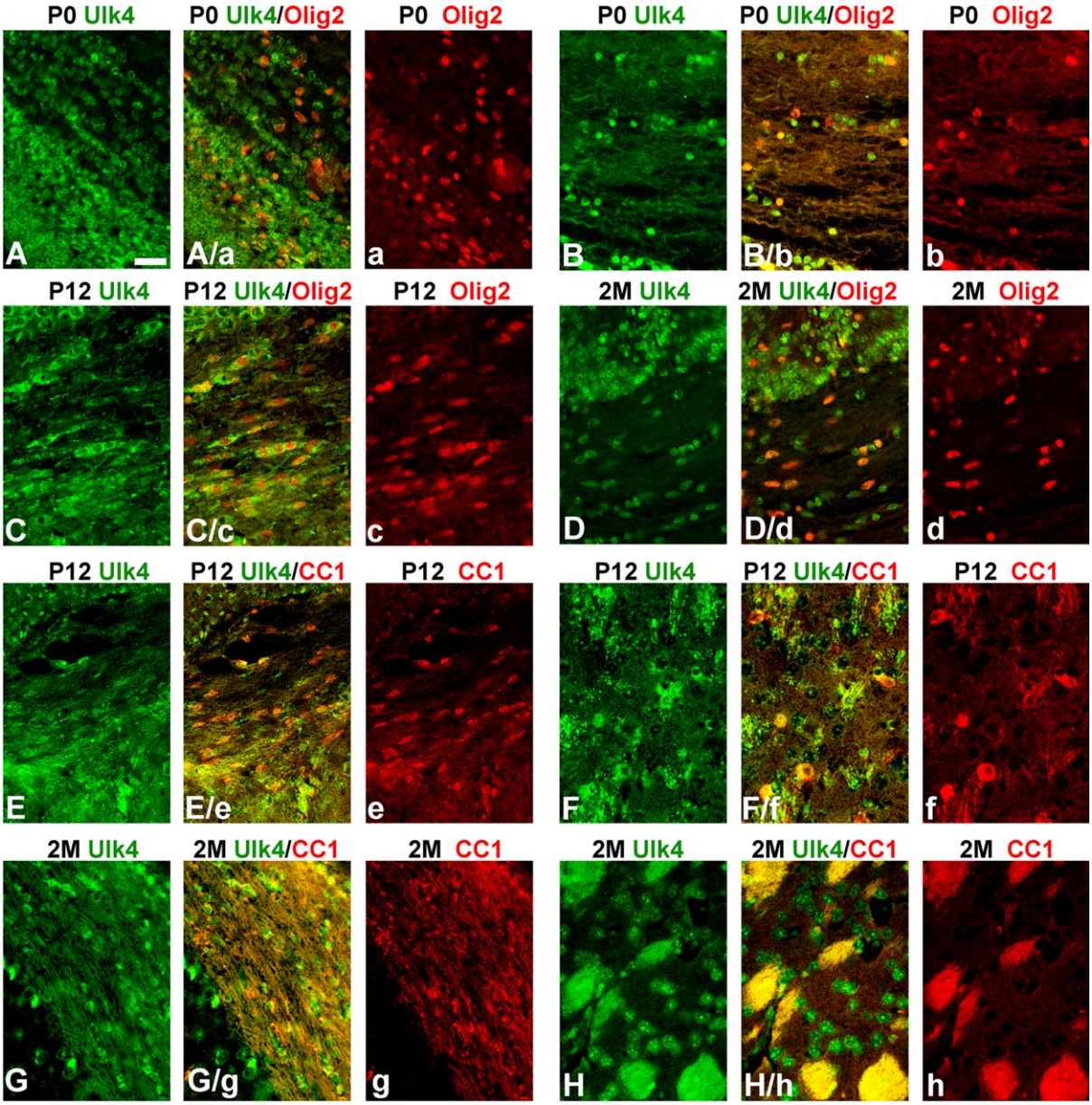

FIGURE 1 Ulk4 is expressed in oligodendrocyte lineage during development. P0 (A-B, a-b), P12 (C,E-F, c,e-f) and 2-month (D,G,H, d,g,h) mouse brain sections were immune-stained with anti-Ulk4 (A-H) and a nti - Olig2 (a-d) for all oligodendrocyte lineage, or with anti-Ulk4 and CC1 (e–h) for mature oligodendrocytes. Note that all Olig2$^+$ cells were Ulk4$^+$ in the P0 SVZ (A/a), and CC of P0 (B/b), P12 (C/c) and 2-month (D/d) brain, and all CC1$^+$ oligodendrocytes in P12 CC (E/e) and cortex (F/f), and in 2-month CC (G/g) and thalamic nerve fibers (H/h) were co-stained with anti-Ulk4. Scale bar = 20μm in A–H

co-localization of CC1$^+$ activity in Ulk4$^+$ cells in P12 CC (Figure 1E/e), P12 cortex (Figure 1F/f), 2-month CC (Figure 1G/g) and thalamic nerve fibers (Figure 1H/h). Thus, the anti-Olig2 and CC1 immuno-reactivity are co-localized with anti-Ulk4, suggesting that Ulk4 is expressed in all developmental stages of oligodendrocytes.

3.2 | Reduced Olig2$^+$ cells in the CC of P12 *Ulk4*$^{tm1a/tm1a}$ mice

The CC is a formed by axon bundles projected from cortical neurons and connects left and right cerebral hemispheres. Defects of the CC integrity and/or CC agenesis are common in neurodevelopmental and neuropsychiatric disorders including schizophrenia and ASD (Chinnasamy et al., 2006; Innocenti et al., 2003; Motomura et al., 2002; Paul et al., 2007; Swayze et al., 1997; Wolf et al., 2008; Wolff et al., 2015) in which ULK4 CNVs are associated with (Lang et al., 2014; Liu, Guan, Shen, Flinter, et al., 2016). We subsequently investigated Olig2$^+$ cell population in WT and *Ulk4*$^{tm1a/tm1a}$ CC to access the oligodendrocyte development at P12, as most *Ulk4*$^{tm1a/tm1a}$ mutants died before weaning (Liu, Guan, Shen, Lalor, et al., 2016). In both the middle (Figure 2b) and lateral (Figure 2d) parts of the CC, Olig2$^+$ cells were markedly reduced in the *Ulk4* mutants (Figure 2a,c), although the total cell

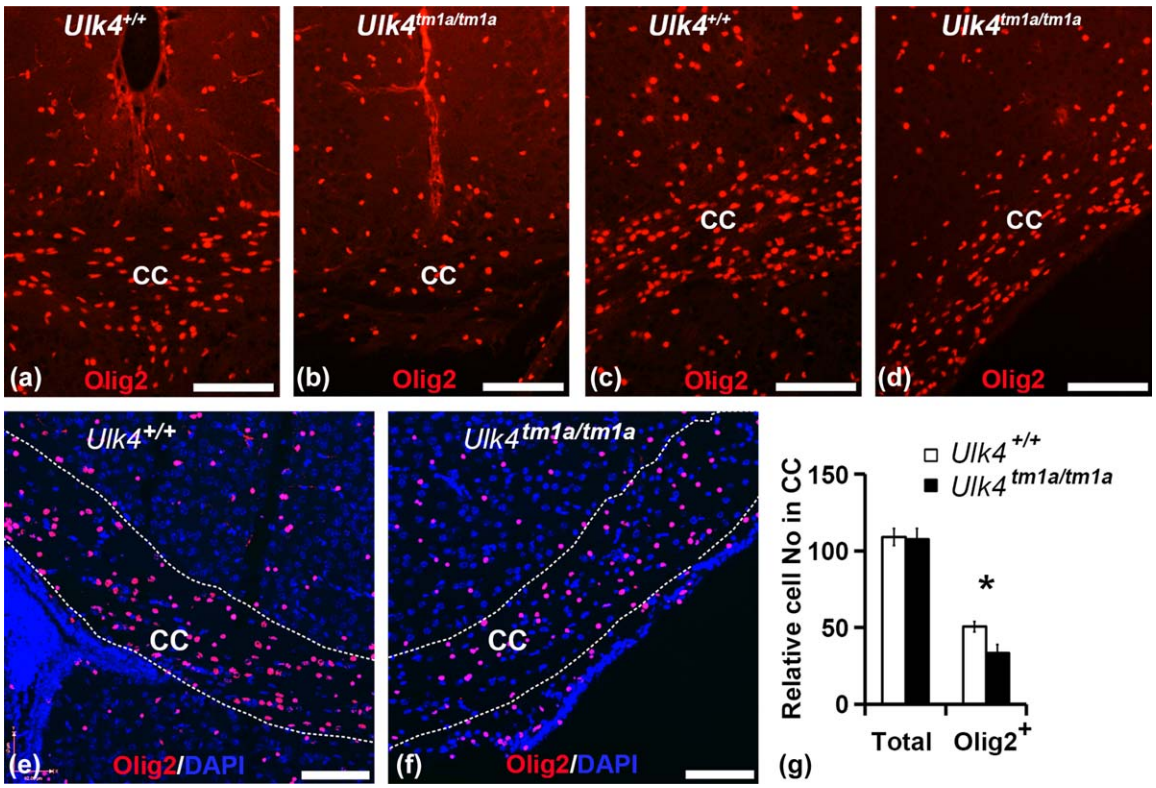

FIGURE 2 Anti-Olig2 staining showed a significant reduction of Olig2$^+$ cells in the CC of *Ulk4*$^{tm1a/tm1a}$ mice. P12 brain sections from WT littermate controls (a, c, e) and *Ulk4*$^{tm1a/tm1a}$ mice (b, d, f) were stained with anti-Olig2. Images were sampled from the dorsal (a, b, e, f) and lateral CC (c, d). The number of Olig2$^+$ cells was quantified in defined areas (500 μm x 100 μm) in e and f, and showed a loss of 17% Olig2 positive cells in *Ulk4*$^{tm1a/tm1a}$ mice (g, n = 4). WT total nuclei 108.9 ± 5.5, *Ulk4*$^{tm1a/tm1a}$ total nuclei 108.9 ± 5.5; WT Olig2$^+$ cells 50.6 ± 3.3, *Ulk4*$^{tm1a/tm1a}$ Olig2$^+$ cells 33.3 ± 5.8 (d, m ± SEM). Bar = 100 μm in A-F, * for $p < 0.05$

number of the regions remained unchanged between two genotypes (Figure 2e–g). Quantification of Olig2$^+$ cells showed a ~17% reduction in the comparable regions of mutant CC (Figure 2e–g).

Next we quantified other glial cells in the brain using anti-Gfap (Figure 3a-d′) for astrocytes and anti-Iba1 for microglia. *Gfap* was the most significantly altered molecule among the 19,652 transcriptome, with a 2.86-fold induction in *Ulk4*$^{tm1a/tm1a}$ brain. Gfap$^+$ astrocytes were significantly increased in the anterior CC of *Ulk4* mutants (49.1 ± 5.0%, n = 3, $P = 0.04$, Figure 3d) compared with that in WT controls (28.4 ± 1.9%, n = 4, Figure 3c). In the posterior CC, the Gfap$^+$ cells were also markedly increased in mutants (Figure 3a,b).

As both progenitors of oligodendrocyte and astrocyte lineages are known to express Olig2 (Chen et al., 2008), we next performed double staining with anti-Olig2 and anti-Gfap (Figure 3c-d′). The lack of Olig2$^+$/Gfap$^+$ co-labeling demonstrated that reduced Olig2$^+$ oligodendrocytes were not a consequence of increased astrocyte production in the mutant CC. Examination of higher magnification images showed reactivated morphology of astrocytes in *Ulk4*$^{tm1a/tm1a}$ brain, with enlarged cell bodies and thicker processes (Figure 3d′), while WT brain showed resting astrocytes with lightly stained cell body and thin processes predominantly in the CC and cortex (Figure 3c′). The same was observed at the hippocampal level (Figure 3a,b).

Astrocytes can be reactivated during neuroinflammation, which is common in hydrocephalic animals (Takei, Shapiro, Hirano, & Kohn, 1987). Microglia are the most sensitive sensors of brain pathology, and undergo a complex and multistage activation process to convert into "activated microglial cells" upon detection of CNS lesion or dysfunction (Kettenmann, Hanisch, Noda, & Verkhratsky, 2011). We recently demonstrated that *Ulk4*$^{tm1a/tm1a}$ mice were impaired in CSF flow (Liu, Guan, Shen, Lalor, et al., 2016), and therefore performed anti-Iba1 staining for microglia to further evaluate neuroinflammation in *Ulk4* mutants (Figure 3e–h′). The Iba1$^+$ cells in the superficial cortex exhibited a typical ramified morphology of resting microglia in both *Ulk4*$^{tm1a/tm1a}$ (Figure 3f) and controls (Figure 3e), with no significant change in cell number or morphology. In the deep cortical layers and CC, however, Iba1$^+$ cells became large amoeboid with round cell body but reduced processes in *Ulk4*$^{tm1a/tm1a}$ mice (Figure 3h,h′) compared with WT mice (Figure 3g,g′). Together these data suggests a high degree of neuroinflammation in the *Ulk4*$^{tm1a/tm1a}$ mice.

3.3 | Reduced myelination in the *Ulk4*$^{tm1a/tm1a}$ mice

Mbp is a myelin marker for mature oligodendrocytes, and we next investigated myelination at P12, by anti-Mbp staining. Mbp was abundantly expressed in myelinated fiber tracks of the WT CC (Figure 4a), however, the anti-Mbp staining was restricted to the most dorsal part of the CC in P12 *Ulk4*$^{tm1a/tm1a}$ brain (Figure 4d), which was projected by primary motor cortex in the vicinity of dorsal midline of the cortex

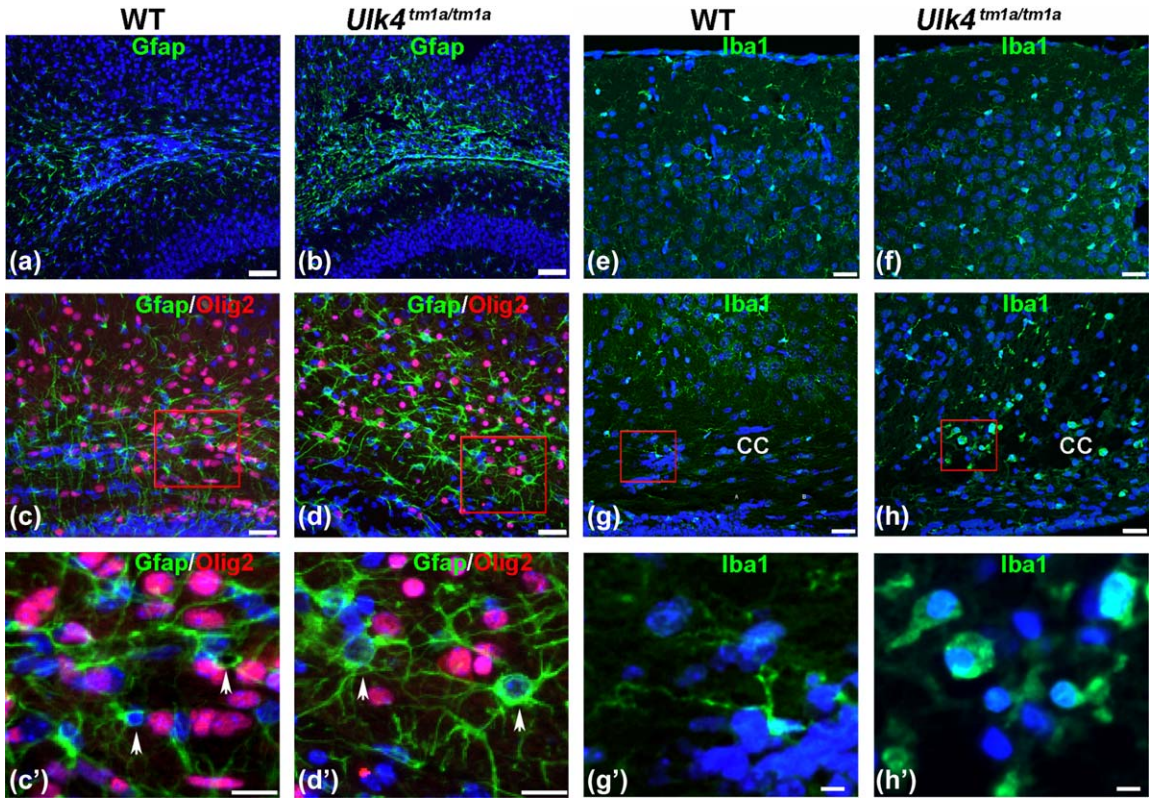

FIGURE 3 Elevated neuroinflammation in P12 *Ulk4*$^{tm1a/tm1a}$ mice. Coronal sections of WT (a, c, c′, e, g, g′) and *Ulk4*$^{tm1a/tm1a}$ (b, d, d′, f, h, h′) brain were stained with anti-Gfap for astrocytes (green, a-d′), anti-Olig2 for oligodendrocytes (red, c-d′), anti-Ibal for microglia (green, e-h′), and DAPI for nuclei (blue). Images in a and b were from the hippocampal level showing reactivated astrocytes in the mutant (b). Images in c and d were sampled from the CC adjacent to the lateral ventricle, and c′ and d′ were the higher magnification images of c and d respectively. Arrows in d′ showing activated astrocytes with larger cell bodies and more projection. Images in e and f were taken from the superficial layers and in g and h from the deep cortical layers. Images in g′ and h′ were magnified view of the boxed areas in g and h, respectively, showing activated microglia with enlarged cell bodies in deep cortical layers of *Ulk4*$^{tm1a/tm1a}$ mice (h′). Note that increased reactivated Gfap+ cells were present in both the anterior (d) and posterior parts (b) of *Ulk4*$^{tm1a/tm1a}$ CC compared to the WT controls (c, a). There was no co-labeling of anti-Olig2 and anti-Gfap in WT or *Ulk4*$^{tm1a/tm1a}$ mice. Scale bar =100μm in a–h; 20 μm in g′ and h′; 50 μm in c′ and d′. * for $p < 0.05$, and ** for $p < 0.01$

(Zhou et al., 2013). In the dorsal lateral ependymal region, the myelinated projections from the cortex were dramatically reduced in the mutants (Figure 4e) compared to WT controls (Figure 4b). In the SVZ region, myelinated axonal bundles were densely projected from the lateral cortex to the thalamus in WT (CPU, Figure 4c), but they were missing in the mutants. The myelin in other brain regions, such as deep cortex (CX, Figure 4b,c,e,f) was also markedly reduced. These data demonstrated a significant reduction of myelin in P12 *Ulk4*$^{tm1a/tm1a}$ mice.

To determine if *Ulk4*$^{tm1a/tm1a}$ mice could catch up myelination at a later stage, we investigated the P18 mice by TEM (Figure 4g–j). The TEM images were taken from the comparable CC region, and examination of 536 axons from 3 WT ("m" in Figure 4g) and 1299 axons from three mutant images ("m" in Figure 4h) showed 57.5 ± 3.5% myelinated axons in the WT, but 26.2 ± 5.9% ($p < 0.01$) in the *Ulk4*$^{tm1a/tm1a}$ mice (Figure 4l). The myelin thickness on the myelinated axons was mildly reduced from 133.9 ± 4.5 nm in WT to 99.8 ± 5.8 in *Ulk4* mutants ($p < 0.01$, Figures 3i,j,m). Therefore, TEM data support a significant decrease in both the myelinated axon number and the myelin production in P18 *Ulk4*$^{tm1a/tm1a}$ mice.

We next quantified the *Mbp* transcripts against *Nefh*, an axon skeleton molecule involved in the mutual sustenance of axons and myelin, and a marker commonly used for neuronal damage in amyotrophic lateral sclerosis(Larsen, DaSilva, Conant, & Yong, 2006). A∼50% reduction of *Mbp* mRNA was detected in the *Ulk4* mutants (Figure 4k). In contrast, there was no difference on *Nefh* mRNA between WT and *Ulk4* mutants (101%, $p = 0.47$). Neither was there a significant change on *Nefl* (101%, $p = 0.47$) or *Nefm* (95%, $p = 0.36$) transcription (Figure 4k). In addition, *Mbp* mRNA transport in oligodendrocytes appeared normal, and transcripts of *Ckap5*, encoding a microtubule-associated protein for transport of *Mbp* mRNA from cell body to the myelin compartment (Maggipinto et al., 2017), is 111% increased in *Ulk4*$^{tm1a/tm1a}$ mice ($p = 5.98E\text{-}08$, FDR = 1.44E-06). Therefore, the myelin, not the axonal skeleton molecules, was specifically reduced by *Ulk4* lesion.

Axon-derived factors and axon size can regulate oligodendroglial development and myelination, and signals associated with axonal

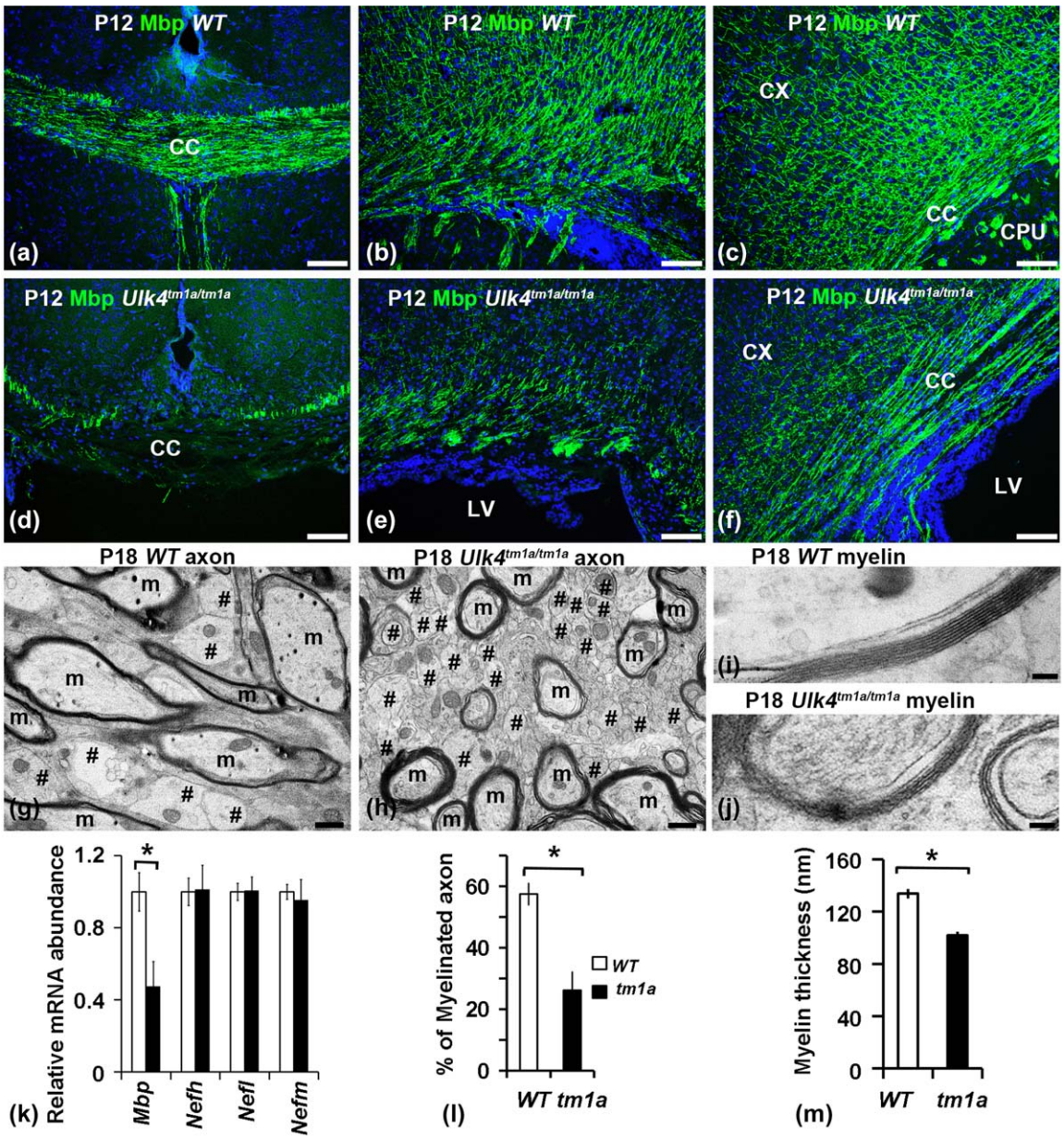

FIGURE 4 *Ulk4*$^{tm1a/tm1a}$ mice exhibited hypomyelination in cortex and CC. Immunohistochemical staining of P12 WT (a–c) and *Ulk4*$^{tm1a/tm1a}$ (d–f) brain sections with anti-Mbp showed dense and directional myelinated nerve fibers in the WT CC and cortex (a–c), and the CC and cortex in *Ulk4*$^{tm1a/tm1a}$ brain (d–f) showed a dramatic reduction in anti-Mbp staining. (g–j) TEM images of axons (g,h) and myelin (i,j) from P18 WT (g,i) and *Ulk4*$^{tm1a/tm1a}$ (h,j) mice. (k) Relative mRNA expression of the Mbp, Nefh, Nefl and Nefm genes in WT (hollow bars) and *ULk4*$^{tm1a/tm1a}$ (solid bars) brain showing specific reduction of Mbp. (l) Quantification of the axons from 10,000-time magnified images of the respective CC region showed 308/536 (57.5 ± 3.5%) myelinated axons in P18 WT, and 340/1299 (26.2 ± 5.9%, $p < 0.01$, $n = 3$) in the *Ulk4*$^{tm1a/tm1a}$ mice. (m) The thickness of myelin on the myelinated axons was 133.9 ± 4.5 nm in 3 WT and 99.8 ± 5.8 in 3 *Ulk4*$^{tm1a/tm1a}$ mice ($p < 0.01$). Bar = 100 μm in a–f, 500 nm in g-h, 100 nm in i-j. CC, corpus callosum; CPU, caudate putamen; CX, cortex; LV, lateral ventricle. "m" for myelinated axons, "#" for unmyelinated axons.* for $p < 0.05$

degeneration may also induce oligodendrocyte proliferation (Sun et al., 2010). We further examine myelination on TEM images. Many areas of mutant CC were showed to lack axons at P18 (#, Figure 5b), and in contrast, the WT CC was densely packed with axons (Figure 5a). Smaller axons were also observed in the *Ulk4*$^{tm1a/tm1a}$ CC (Figures 5b, d). Quantification of the myelinated axons from the TEM images demonstrated that both the inner and outer diameters of axons were significantly smaller in *Ulk4* mutants compared with WT littermates (Figures 5e–f,h, $p < 0.05$), whereas the *G* ratio (inner/outer diameter) was not altered (Figure 7g,i, $p = 0.455$). Therefore, myelination thickness appears to be in proportion to the axon size in both genotypes. These data thus provided strong evidence of fewer myelinated axons and decreased axon caliber in *Ulk4*$^{tm1a/tm1a}$ mice, which might exert secondary effects on the reduced myelination.

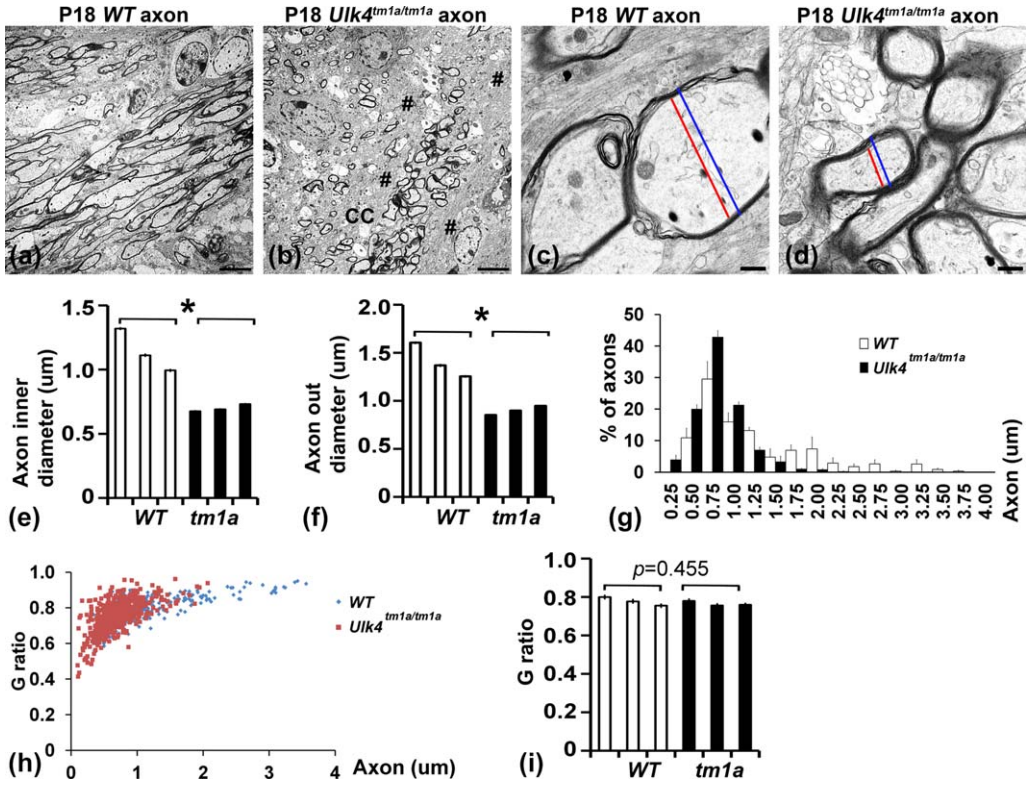

FIGURE 5 Reduced axonogenesis in *Ulk4*$^{tm1a/tm1a}$ mice. (a-d) TEM images of WT (a,c) and *Ulk4* mutant (b,d) CC, showing areas (#, b) lacking axon and reduced axon size (d) in the mutants. Bar = 5 μm in A-B, 500 nm in c-d. The axon size was quantified from 80, 72 and 102 axons in three WT and 67, 107 and 123 axons from three mutants. The inner (red line in c and d) and outer (blue line in c and d) diameters were measured from the narrower plan for on-round shaped axons. The myelin thickness was half of the difference of outer and inner diameters. (e) The inner diameter of axons was 1141.5 ± 95.2 nm in WT and 699.8 ± 13.0 in *Uik4*$^{tm1a/tm1a}$ mice (p = 0.01). (e) The axon outer diameter was reduced from 1409.2 ± 103.3 nm in WT to 899.8 ± 20.8 in *Uik4*$^{tm1a/tm1a}$ mice ($p < 0.01$). (g) Myelinated axon diameter distributions of *Ulk4*$^{tm1a/tm1a}$ and *Ulk4*$^{+/+}$ mice ($n = 3$). Columns represent percentage (%) of axons (mean ± SEM, $n = 3$ animals in each group), showing *Ulk4*$^{tm1a/tm1a}$ mutant axons are more concentrated at the smaller size range (x^2=40, $p < 0.01$). (h) Plot of pooled G ratio against axon diameter for *Ulk4*$^{tm1a/tm1a}$ and *Ulk4*$^{+/+}$ mice ($n = 3$). mice ($n = 3$). (i) The G ratio (inner/outer diameter) was unchanged between WT (0.78 ± 0.01) and mutants (0.77 ± 0.01, $p = 0.455$). * for $p < 0.05$; ** for $p < 0.01$

3.4 | Reduced expression of oligodendrocyte-lineage enriched genes in the *Ulk4*$^{tm1a/tm1a}$ mice

Oligodendrogenesis is regulated by both intracellular transcriptional factors and extracellular signals (Emery, 2010; Nicolay et al., 2007). Previous transcriptome analyses showed continuous changes from P18, P75 to 6-month in C57BL/6N mice, suggesting that myelin transcriptome reaches a stable state by 6 months (Thakurela et al., 2016). To gain a full picture of myelination in the *Ulk4* mutants, we carried out whole genome RNA sequencing in P12 cortex, the middle stage of postnatal oligodendrogenesis with all kinds of oligodendrocytes present. Quantitative reads of 19,652 transcripts were acquired from P12 cortex and normalized to FPKM.

We first targetedly analyzed the transcriptome by cross-examination with oligodendrocyte transcriptome identified in two recent studies (Thakurela et al., 2016; Zhang et al., 2014), in which 40 most abundant genes, 20 enriched transmembrane receptors, 20 top ligands and 10 most abundant transcription factors were identified for the OPCs, the newly formed oligodendrocytes (NFOs) and myelinating oligodendrocytes (MOs), respectively (Table 1). Whereas none of the top 10 TFs was upregulated in *Ulk4* mutants, six OPC transcription factors (*Olig1*, *Sox10*, *Olig2*, *Sox8*, *Sox6*, *Nkx2-2*), seven NFO transcription factors (*Olig1*, *Myrf*, *Sox10*, *Olig2*, *Sox8*, *Nkx6-2*, *Nkx2-2*) and five MO transcription factors (*Olig1*, *Sox10*, *Sox8*, *Carhsp1*, *Nkx6-2*) were significantly reduced (Supporting Information Table I). Among the 40 most abundant genes, 3 were downregulated in OPCs, 24 in NFOs and 22 in MOs, respectively (Supporting Information Table II). In addition, out of the top 20 transmembrane receptors and 20 ligands, 9 OPC, 21 NFO and 21 MO genes were significantly down-regulated (Supporting Information Table III). These data suggest a mild change of transcriptome in OPCs, but more dramatic reductions of NFOs and MOs in *Ulk4* mutants.

3.5 | A Systematic disruption of the myelination network in the *Ulk4*$^{tm1a/tm1a}$ mice

We subsequently analyzed the transcriptome data with multiple testing P-value and FDR (false discovery rate), and myelination pathways were notably enriched in *Ulk4* mutants. Among the 100 most significantly

TABLE 1 Altered oligodendrocyte-lineage gene expression in *Ulk4* mutants

Cell population	Most abundant genes	Significantly downregulated genes in *Ulk4* mutants	Significantly upregulated genes in *Ulk4* mutants
OPCs	10 TFs	6 (*Olig1*, *Sox10*, *Olig2*, *Sox8*, *Sox6*, *Nkx2-2*)	None
OPCs	40 enriched genes	3 (*Col1a2*, *Mmp15*, *Cspg4*)	4 (*Rasgrf1*, *Slitrk1*, *Ncald*, *Cdo1*)
OPCs	20 TM receptors	4 (*Gpr17*, *Plxnb3*, *Sema5a*, *Il1rap*)	6 (*Gabra3*, *Omg*, *Oprl1*, *Lypd1*, *Adora1*, *Gria3*)
OPCs	20 ligands	5 (*Gsn*, *Il1rap*, *Igsf21*, *Gpc5*, *Scrg1*)	3 (*Nptx2*, *C1ql3*, *Dscam*)
NFOs	10 TFs	7 (*Olig1*, *Myrf*, *Sox10*, *Olig2*, *Sox8*, *Nkx6-2*, *Nkx2-2*)	None
NFOs	40 enriched genes	24 (*Nfasc*, *Tns3*, *Enpp6*, *9630013A20Rik*, *Rnf122*, *Cnksr3*, *Gp1bb*, *Lims2*, *1810041L15Rik*, *Sema5a*, *Fyn*, *Elovl6*, *Slc12a2*, *Frmd4a*, *Kif19a*, *Chn2*, *Itpr2*, *Tmem163*, *Rras2*, *Pik3r3*, *Ust*, *Samd4b*, *Mical3*, *Fmnl2*)	3 (*Cyfip2*, *Fam73a*, *Atrn*)
NFOs	20 TM receptors	12 (*Gpr17*, *Sema4d*, *Plxnb3*, *Ephb1*, *Lpar1*, *Gpr37*, *S1pr5*, *Sema5a*, *Il1rap*, *Prkcz*, *Casr*, *Erbb3*)	1 (Omg)
NFOs	20 ligands	9 (*Gsn*, *Adamts4*, *Enpp6*, *Metrn*, *Il1rap*, *Col11a2*, *Lgi3*, *Elfn2*, *Scrg1*)	1 (*Dscam*)
MOs	10 TFs	5 (*Olig1*, *Sox10*, *Sox8*, *Carhsp1*, *Nkx6-2*)	None
MOs	40 enriched genes	22 (*Mbp*, *Cldn11*, *Kif5a*, *Mal*, *Mog*, *Gsn*, *Trp53inp2*, *Trf*, *Plekhb1*, *Prr18*, *Opalin*, *Inf2*, *Trak2*, *Tbc1d9b*, *Ppp1r14a*, *Gjb1*, *Cryab*, *Nol3*, *Cdc42ep2*, *Pdlim2*, *Slc45a3*, *Efhd1*)	2 (*Ndrg1*, *Apod*)
MOs	20 TM receptors	11 (*Gpr17*, *Sema4d*, *Plxnb3*, *Ephb1*, *Lpar1*, *Gpr37*, *S1pr5*, *Sema5a*, *Il1rap*, *Prkcz*, *Erbb3*)	1 (*Omg*)
MOs	20 ligands	10 (*Gsn*, *Trf*, *Adamts4*, *Enpp6*, *Metrn*, *Il1rap*, *Col11a2*, *Lgi3*, *Il23a*, *Erbb3*)	1 (*Apod*)

dysregulated genes with FDR <9.524E-33, 37 genes are myelination-related (Table 2). Remarkably, among the top 30 dysregulated genes, 20 genes (*Gfap*, *Mbp*, *Mobp*, *Plp1*, *Slc1a2*, *Ttr*, *Cnp*, *Scd2*, *Nfasc*, *Mag*, *Ptgds*, *Cldn11*, *Atp1a2*, *Spp1*, *Sirt2*, *Ugt8a*, *Tspan2*, *Bcas1*, *Gpr17* and *Snap25*) are myelin-related, and 17 of them were down-regulated in the *Ulk4* mutants. The Mbp, Mobp, Plp1 and Cnp are the most abundant myelin components in the CNS, and they are ranked as 2nd, 3rd, 4th and 8th most significantly altered genes among the 19,652 transcripts, with 45–56% reduction in the *Ulk4*$^{tm1a/tm1a}$ cortex. The membrane proteins Nfasc (37%↓), Mag (49%↓), Cldn11 (48%↓), Tspan2 (40%↓) and Gpr17 (38%↓) are decreased, which are involved in cell adhesion, cell interactions, tight junctions, oligodendrocyte terminal differentiation and maturation, respectively. Cytoskeleton modification molecules Sirt2 (36%↓, which deacetylates α-tubulin at Lys-40 during OPC differentiation) and Bcas1 (45%↓, a novel myelin-associated protein interacting with F-actin and the dynein light chain are also decreased. The enzyme Scd2 (28%↓) involved in lipid synthesis and Ugt8a (48%↓) in sphingolipid synthesis are reduced. A secreted remyelination-enriched phosphoprotein Spp1 (28%↓) is down-regulated (Selvaraju et al., 2004). Hypomyelination is, thus, the most striking phenotype in *Ulk4*$^{tm1a/tm1a}$ mutants.

The *Ulk4* targets were narrowed to 618 genes with a $p < 0.05$; FPKM > 1, >20% reduction or >1.5-fold increase, which were analyzed by the STRING program (http://string-db.org/). Series of myelination pathways were identified, and most significantly, all were downregulated in mutants (Figure 6). For example, eight genes in the "Oligodendrocyte differentiation" pathway (*Cnp*, *Dusp10*, *Fa2h*, *Myrf*, *Olig2*, *Plp1*, *Sox10* and *Tspan2*) were decreased by 23%–50% (Figure 6b); 17 "regulators of oligodendrocyte differentiation and maturation" including *Olig2*, *Olig1*, *Sox10*, *Myrf*, *Hdac2*, *Sirt2* and *Dusp10* were significantly downregulated (Figure 6d, $p < 0.05$); 12 "Myelination" genes (*Arhgef10*, *Fa2h*, *Gal3st1*, *Gjc3*, *Myrf*, *Mbp*, *Nfasc*, *Olig2*, *Plp1*, *Sirt2*, *Tspan2* and *Ugt8a*) were downregulated by 30%–53% (Figure 6a, $p < 0.05$); and 18 "Myelin sheath" genes (*Atp1a2*, *Car2*, *Cldn11*, *Cnp*, *Ermn*, *Gjc2*, *Gjc3*, *Mag*, *Mbp*, *Mobp*, *Mog*, *Myo1d*, *Nfasc*, *Pllp*, *Plp1*, *Rap1a*, *Sirt2* and *Tspan2*) were reduced by 23%–56% (Figure 6c). The RNA sequencing data therefore overwhelmingly support the immunohistochemical and TEM data for a systematic hypomyelination in the *Ulk4*$^{tm1a/tm1a}$ mice.

3.6 | Impaired oligodendrocyte development in *Ulk4*$^{tm1a/tm1a}$ mice

Oligodendrogenesis is divided into 5 stages with overlapping markers (Mattan et al., 2010) (Figure 7a,b). The transcription factors Id2, Id4, Hes5 and Sox6 are required to maintain OPCs and to repress myelin gene expression. They were not significantly altered in *Ulk4*$^{tm1a/tm1a}$ mice, suggesting that Ulk4 had no overt effect on myelin repressors.

The expression of *Cspg4* encoding Ng2, a typical marker for pro-oligodendrocytes, was decreased by 17% in *Ulk4*$^{tm1a/tm1a}$ mice. *Olig1*, *Nkx2-2* and *Sox10*, required for the generation of post-mitotic oligodendrocytes (Menet, Prieto, Privat, & Ribotta, 2003), were downregulated by 30%–34%. *Myrf*, expressed by post-mitotic oligodendrocytes and induced concurrently with terminal differentiation (Cahoy et al., 2008), was reduced by 38%. Two other NFO markers,

TABLE 2 Top 37 myelin-related genes among the 100 most significantly dys-regulated genes in *Ulk4* mutants

Significance (order)	Gene (symbol)	FPKM (Mean± SEM); (WT)	FPKM (Mean ± SEM); (*Ulk4* mutant)	*P*-value	FDR	Ratio (Mutant/WT)
1	*Gfap*	62.8 ± 7.4	179.6 ± 47.7	0.000E+00	0.000E+00	2.86
2	*Mbp*	2775.7 ± 298.0	1318.2 ± 386.5	0.000E+00	0.000E+00	0.47
3	*Mobp*	212.1 ± 14.4	93.1 ± 33.5	0.000E+00	0.000E+00	0.44
4	*Plp1*	927.9 ± 54.3	506.5 ± 136.3	0.000E+00	0.000E+00	0.55
5	*Slc1a2*	604.0 ± 20.9	462.7 ± 27.5	0.000E+00	0.000E+00	0.77
6	*Ttr*	388.1 ± 177.8	32.9 ± 28.5	0.000E+00	0.000E+00	0.08
8	*Cnp*	225.6 ± 19.7	118.5 ± 34.1	1.202E-232	2.625E-229	0.53
9	*Scd2*	321.4 ± 23.2	231.3 ± 31.1	4.737E-215	9.309E-212	0.72
12	*Nfasc*	67.3 ± 3.1	42.7 ± 7.9	1.061E-150	1.604E-147	0.63
13	*Mag*	129.6 ± 8.4	66.5 ± 20.4	3.225E-148	4.527E-145	0.51
14	*Ptgds*	297.7 ± 51.6	534.6 ± 32.4	4.704E-140	6.163E-137	1.80
15	*Cldn11*	162.9 ± 6.6	85.2 ± 21.7	1.850E-139	2.272E-136	0.52
16	*Atp1a2*	228.0 ± 10.8	175.5 ± 11.4	1.850E-139	2.272E-136	0.52
20	*Spp1*	11.0 ± 1.5	74.8 ± 4.8	4.244E-102	3.476E-99	0.72
21	*Sirt2*	272.0 ± 27.4	175.2 ± 26.7	1.989E-104	1.776E-101	0.64
22	*Ugt8a*	61.0 ± 3.3	31.4 ± 10.1	2.129E-103	1.819E-100	0.52
24	*Tspan2*	73.0 ± 3.6	44.0 ± 9.7	1.839E-93	1.446E-90	0.60
25	*Bcas1*	85.0 ± 9.1	47.0 ± 14.8	1.434E-92	1.084E-89	0.55
27	*Gpr17*	71.6 ± 7.2	44.1 ± 12.0	2.037E-90	1.430E-87	0.62
29	*Snap25*	744.8 ± 49.5	911.7 ± 111.7	1.427E-83	9.346E-81	1.22
31	*Camk2a*	756.5 ± 12.2	673.2 ± 47.7	1.148E-81	7.050E-79	0.89
36	*Ppp3r1*	240.5 ± 18.7	312.2 ± 32.3	5.286E-64	2.734E-61	1.30
39	*Mal*	72.3 ± 7.3	44.5 ± 12.1	4.152E-61	2.040E-58	0.62
43	*Atp1a1*	292.2 ± 30.6	354.0 ± 34.8	4.325E-58	1.976E-55	1.21
45	*Qk*	109.0 ± 8.2	85.0 ± 8.0	3.918E-55	1.638E-52	0.78
51	*Enpp2*	111.1 ± 15.9	80.2 ± 5.9	2.344E-53	8.857E-51	0.72
58	*Map1b*	173.7 ± 5.4	153.2 ± 7.8	2.821E-49	9.396E-47	0.88
60	*Tubb4a*	514.1 ± 9.5	431.7 ± 15.1	4.701E-48	1.515E-45	0.84
63	*Mog*	60.9 ± 2.4	32.2 ± 8.3	1.055E-46	3.240E-44	0.53
65	*Gsn*	56.1 ± 2.0	33.7 ± 8.7	1.603E-45	4.774E-43	0.60
71	*Hmgcs1*	146.5 ± 6.8	111.5 ± 18.6	8.876E-43	2.423E-40	0.76
73	*Kcnj10*	72.2 ± 8.0	53.3 ± 6.1	1.023E-41	2.717E-39	0.74
75	*Tppp*	114.7 ± 5.7	90.9 ± 12.0	1.622E-41	4.193E-39	0.79
81	*Fa2h*	29.9 ± 1.4	14.9 ± 4.8	5.042E-39	1.208E-36	0.50
87	*Nsf*	174.4 ± 15.1	214.9 ± 9.8	3.114E-38	7.033E-36	1.23
93	*Sema6a*	22.2 ± 2.4	14.1 ± 2.0	4.526E-36	9.462E-34	0.63
99	*Trf*	46.8 ± 2.3	27.7 ± 11.5	4.846E-35	9.524E-33	0.59

Nfasc and *Enpp6*, were decreased by 36% and 48%, suggested a stronger effect of Ulk4 on the birth of post-mitotic oligodendrocytes (Figure 7b). The markers for non-compact myelinating oligodendrocytes, *Sirt2* and *Cnp*, were downregulated by 36% and 47%, and three markers for compact myelinating oligodendrocytes, *Plp1*, *Mbp* and *Ugt8* were downregulated by 45%-53%. The expression of *Mog* (a marker for

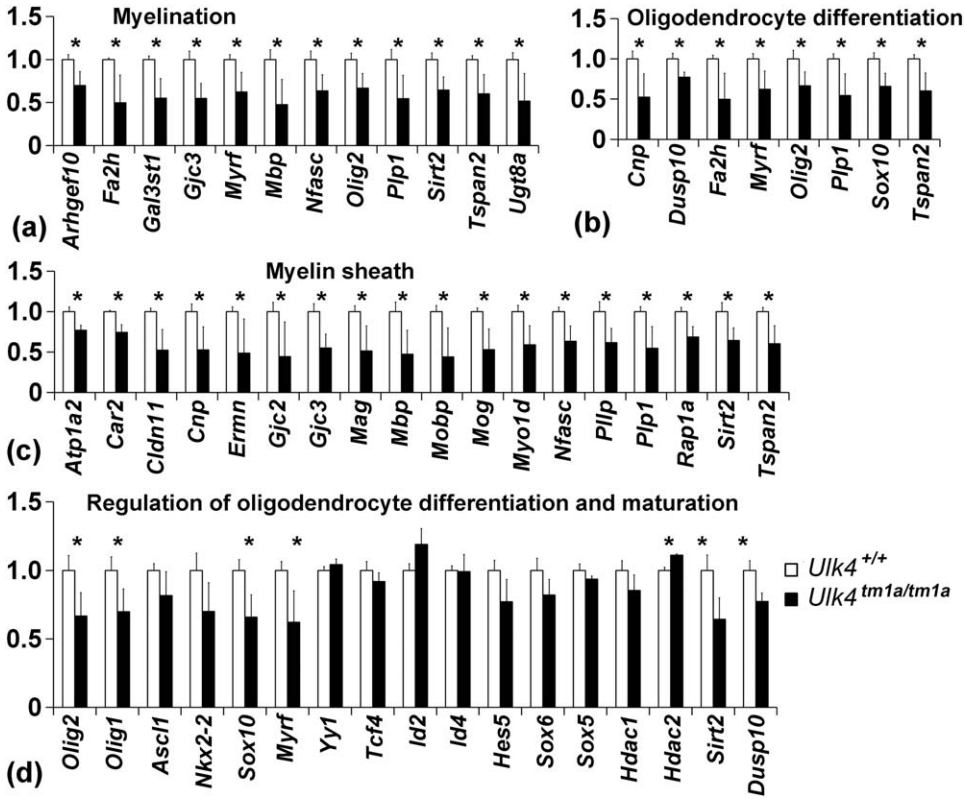

FIGURE 6 Transcriptome analyses showing significant down-regulation of oligodendrogenesis genes in *Ulk4*$^{tm1a/tm1a}$ mice. Significantly altered pathways included "Myelination" (a, $p = 1.59E\text{-}08$), "Myelin sheath" (c, $p = 1.12E\text{-}08$). "Oligodendrocyte differentiation" (b, $p = 2.62E\text{-}06$) and "Regulation of oligodendrocyte differentiation and maturation" (d). * for $p < 0.05$

myelinating mature oligodendrocytes) and *Mag* were downregulated by 47% and 49%, respectively. These data demonstrated a mild effect of Ulk4 on OPCs, a modest effect on NFOs, and much severer effects on maturation of oligodendrocytes.

3.7 | Validation of *Ulk4* targets at the transcriptional and translational levels

We subsequently validated a few key Ulk4 targets in P12 cortical mRNA by quantitative RT-PCR (Figure 7c), which showed 68.6 ± 19.7% of *Olig2* (Figure 7d, $p = 0.13$); 34.2 ± 19.6% of the *Sox17* for immature oligodendrocytes (Figure 7e, $p = 0.01$); 34.9 ± 22.9% of *Mbp* for non-myelinated mature oligodendrocytes (Figure 7f, $p = 0.02$) and 30.8 ± 27.9% of *Mog* mRNA for mature oligodendrocytes (Figure 7g, $p = 0.03$) in *Ulk4* mutants, compared with the WT littermate controls.

Additionally we performed immunoblots with P12 cortical lysate, which further confirmed the reduction of Sox17, Mbp and Mog proteins (Figure 7h–j). Among the three, Sox17 isoforms predicted by the UCSC database (44.6, 38.2 and 30.8 kD), we detected only the 38.2kD protein in P12 mouse cortex, which was reduced to 55.2% in *Ulk4* mutants (Figure 7h, $n = 3$ each, $p < 0.01$). Among the 7 Mbp isoforms predicted (14.2 to 27.2 kD), the 20.3 kD was most abundantly expressed in P12 mouse cortex, which was downregulated to 44.0% in mutants (Figure 7i, $n = 3$ each, $p < 0.01$). Similarly, only the 23.8 kD Mog isoform, not 28.4 kD, was produced by P12 mouse cortex, and this was decreased to 67.9% in *Ulk4* mutants (Figure 7j, $n = 3$ each, $p < 0.05$). These data not only identified the major isoforms of Sox17 (38.2 kD), Mbp (20.3 kD) and Mog (23.8 kD) expressed by P12 cortex, but also confirmed the hypomyelination effect of Ulk4 disruption at both transcriptional and translational levels.

4 | DISCUSSION

Here we present the first evidence that Ulk4 may regulate myelination. Myelin controls the speed of impulse conduction along axons, and synchronized impulse traffic between distant cortical regions is critical for optimal mental performance and learning (Fields, 2008). White matter myelination is therefore suggested as an indicator of functional brain maturation. In healthy individuals, the functional connectivity via the CC increases with myelination from ~4 postnatal months into young adulthood (Giedd et al., 1999). Clinical studies demonstrate that white matter tract and callosal thickness affect cognitive performance, intelligence, processing speed and problem solving in childhood (Hutchinson et al., 2009; Penke et al., 2010; van Eimeren, Niogi, McCandliss, Holloway, & Ansari, 2008). For example, children with developmental delay showed a significant reduction (19.8% of brain volume in patients vs 21.4% in controls, $p < 0.01$) of myelinated white matter (Pujol et al., 2004).

Deficiency of Ulk4 reduces myelin by ~50%, which is significantly higher than 1.6% reduction in children with developmental delay (Pujol

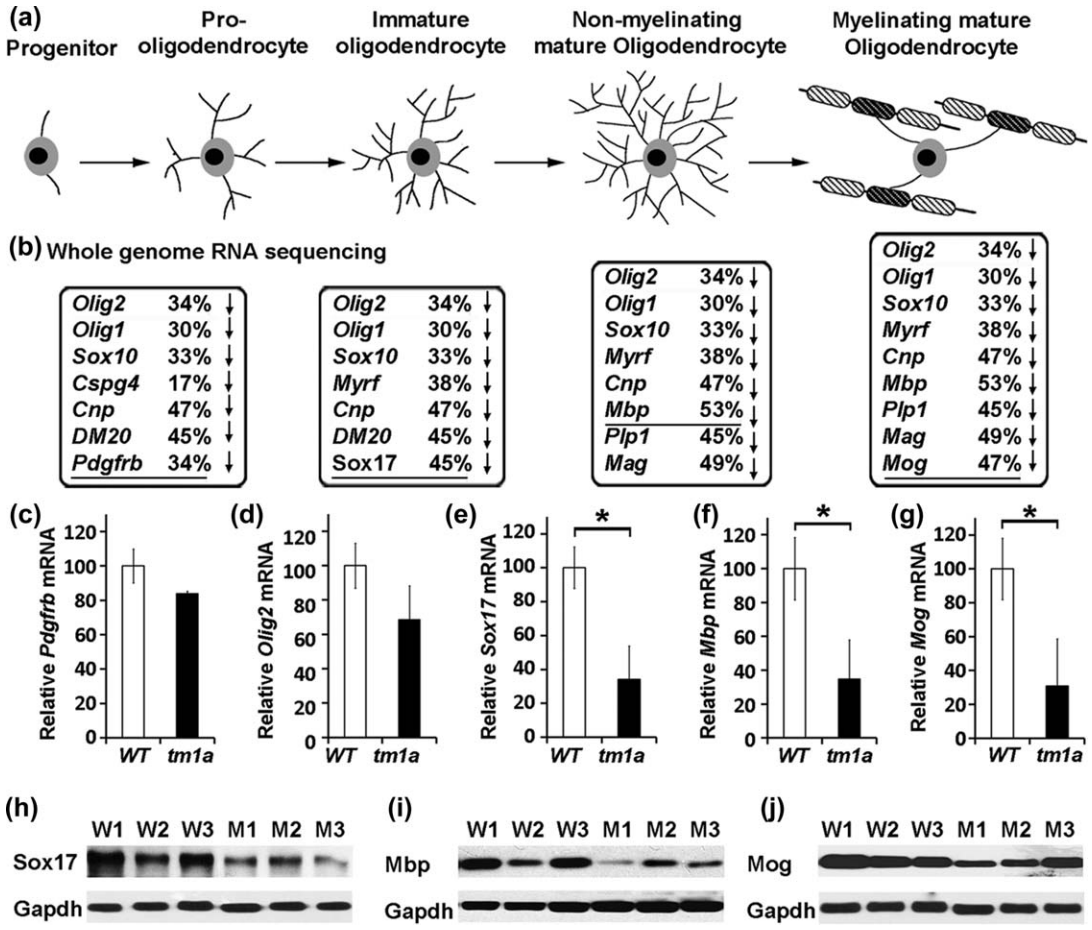

FIGURE 7 Changes in mRNA and protein expression of key genes associated with different stages of oligodendrogenesis in *Ulk4*$^{tm1a/tm1a}$ mice. (a) Five stages of oligodendrocyte development. (b) Whole genome RNA sequencing data from 3 P12 WT and 3 mutant cortical RNA. The abundance of RNA expression was statistically analysed by one-way ANOVA. Data were presented for the key factors related to different stages of oligodendrogenesis with percentage (%) of reduction (↓) in *Ulk4*$^{tm1a/tm1a}$ mice. Underlined were the master regulator *Olig2* and stage-specific markers of *Pdgfrb*, *Sox17*, *Mbp* and *Mog*. (c-g) Validation of mRNA expression by qRT-PCR, showing reduction of mRNA for *Pdgfrb* (WT 100.0 ± 9.9%, mutants 84.0 ± 1.2%, $p = 0.09$); *Olig2* (WT 100.0 ± 13.1%, mutants 68.6 ± 19.7%, $p = 0.13$); *Sox17* (WT 100.0 ± 12.3%, mutants 34.2 ± 19.6%, $p = 0.01$); *Mbp* (WT 100.0 ± 18.4%, mutants 34.9 ± 22.9%, $p = 0.02$); *Mog* (WT 100.0 ± 18.2%, mutants 30.8 ± 27.9%, $p = 0.03$). (h-j) Immunoblotting was carried out with antibodies against Sox17 (h), Mbp (i), Mog (j) and Gapdh, and showed reduction of Sox17 protein from 100 ± 6.1% in WT to in 55.2 ± 7.2% mutants ($n = 3$ each, $p < 0.01$); Mbp protein from 100 ± 10.8% in WT to 44.0 ± 21.8% in mutants ($n = 3$ each, $p < 0.01$); and Mog from 100 ± 5.9% in WT to 67.9 ± 6.1% in mutants ($n = 3$ each, $p < 0.05$)

et al., 2004). This help to explain why some *ULK4* patients present severe learning difficulty and language delay (Liu, Guan, Shen, Flinter, et al., 2016). Schizophrenia-associated myelin-related genes including *CNP*, *ERBB3*, *GSN*, *MAL*, *MAG* (Jungerius et al., 2008), and *Bcas1* gene which display hypomyelination and schizophrenia-like behaviours in mutants (Ishimoto et al., 2017) are all downregulated in *Ulk4* hypomorph mice.

Myelination is known to play a crucial role in white matter integrity, and previous *ULK4* was reported to involve in neuritogenesis and CC integrity (Lang et al., 2014). In this study we demonstrate that Ulk4 regulates a core set of oligodendrogeneic factors, and is critical for the maintenance of OPCs, differentiation and maturation of myelinating oligodendrocytes. Ulk4 deficiency significantly downregulates Olig2, Olig1, Sox10, Sox8, Sox6, Sox17, Nkx2-2, Nkx6-2, Myrf, Carhsp1, Sirt2, and Dusp10.

Myelin is constituted by oligodendrocytes. The oligodendrogenesis in mice starts from ~P5 and ends at ~P20 (Fern, Davis, Waxman, & Ransom, 1998), although recent transcriptome analyses suggest further developmental changes beyond this stage (Thakurela et al., 2016). Oligodendrogenesis is regulated by the master transcription factor Olig2 and other intrinsic factors (Emery, 2010). *Olig2*$^{-/-}$ mice show an absence of the oligodendrocyte lineage (Lu et al., 2002; Zhou, Choi, & Anderson, 2001), and Olig2 mRNA is 33% reduced in *Ulk4* mutants.

OPCs are generated from SVZ cells, and Ulk4 is expressed in the NSCs. The *Ulk4* hypomorph mutants exhibit reduced postnatal NSC pool with compromised Wnt signaling in *Ulk4* newborns (Liu, Guan, Shen, Flinter, et al., 2016). The Wnt signaling appears to play different roles in myelination and remyelination (Guo et al., 2015). The canonical Wnt-receptor-β-Catenin-TCF/LEF cascade is thought responsible for remyelination failure in multiple sclerosis and for persistent hypomyelination in periventricular leukomalacia, by delaying/blocking oligodendrocyte differentiation (Franklin & Gallo, 2014). However, recent studies demonstrate that Wnt/β-Catenin signaling plays distinct roles in

oligodendrogenesis, oligodendrocyte differentiation and myelination during development (Guo et al., 2015) and forced Wnt/β-Catenin activation in postnatal dorsal SVZ NSCs enhanced OPC generation (Azim & Butt, 2011; Azim, Rivera, Raineteau, & Butt, 2014). The reduced Wnt signaling and decreased NSC pool in *Ulk4* newborn mice (Liu, Guan, Shen, Flinter, et al., 2016), therefore, are likely to have a direct effect on oligodendrogenesis.

In this study we demonstrate that anti-Olig2 activity is co-localized with anti-Ulk4 at P0, P12 and 2-month. Ulk4 disruption mildly influences the maintenance of OPCs, as fewer OPC-enriched molecules are altered than that in NFOs and MOs (Supporting Information Tables I-III). Also, a17% decrease of OPC-specific marker *Ng2/Cspg4* mRNA is detected, and similarly, Enpp2, a secreted factor regulating the progression of *Olig2*$^{+}$ cells into OPCs (Yuelling, Waggener, Afshari, Lister, & Fuss, 2012) is 28% reduced. *Hmgcs1*, whose mutation causes OPCs to migrate past their target axons and to fail to express myelin genes (Mathews et al., 2014) is downregulated by 24% in *Ulk4* mutants.

Ulk4 plays a strong role on the birth of post-mitotic oligodendrocytes. For example, expression of *Olig1*, *Nkx2-2*, *Sox10* and *Myrf* are reduced by 30–38% in *Ulk4*$^{tm1a/tm1a}$ mice, and other NFO markers including *Sox17*, *Nfasc* and *Enpp6* are decreased by 34–48%. *Myrf* is a marker for post-mitotic oligodendrocytes and vital for generation and maintenance of myelination (Bujalka et al., 2013). Inactivation of *Myrf* causes oligodendrocyte differentiation to stall at an early premyelinating stage. Conversely, forced expression of *Myrf* causes OPCs to express myelin proteins (Cahoy et al., 2008). The *Olig1*, *Nkx2-2*, *Sox10* transcription factors are required for generating post-mitotic oligodendrocytes (Menet, Prieto, Privat, & Ribotta, 2003).

Oligodendrocyte maturation is markedly regulated by Ulk4. For example, Olig1 promotes oligodendrocyte maturation through regulation of Gpr17 (Chen et al., 2009), and in mutants, the expression of Olig1 and Gpr17 is reduced by 30% and 38%, respectively. Enzymes involved in myelin synthesis, such as Scd2 (28%↓) for long-chain unsaturated fatty acids (Schaerenwiemers, Schaefer, Valenzuela, Yancopoulos, & Schwab, 1995), and *Fa2h* (50%↓) for myelin galactolipids containing hydroxy fatty acid are decreased. Mutations in the *FA2H* gene cause leukodystrophy and neurodegeneration, and *Fa2h* deletion in mice caused significant demyelination and profound axonal loss (Potter et al., 2011). Cytoskeleton modification molecules Sirt2 for α-tubulin deacetylation, Tppp for promoting tubulin polymerization (Lehotzky et al., 2010), and Bcas1 for binding F-actin and the dynein light chain are all decreased.

The role of Ulk4 in oligodendrocyte maturation is further strengthened by reduced non-compact myelin markers of *Cnp* (47%) and *Sirt2* (36%), and compact myelin markers of *Plp1* (45%), *Mbp* (53%), *Mobp* (56%) and *Mog* (47%). Cnp mediates early events of myelinogenesis, in particular the elaboration of oligodendrocyte processes. The abundance of Sirt2 and Map1b are controlled by the Qk - Plp pathway in CNS myelin (Zhao et al., 2006; Zhu et al., 2012) and all 4 genes are significantly downregulated. The enzyme Scd2 (28%↓) for lipid synthesis and Ugt8a (48%↓) for sphingolipid synthesis are reduced.

Mbp, Mobp and Plp1 are the major myelin components. Mag is involved in glial-axon interactions during myelination(Marcus, Dupree, & Popko, 2002), and Cldn11 is interlamellar tight junction unique to CNS myelin (Denninger et al., 2015). Mog is located on the surface of oligodendrocytes and myelin sheaths (Brunner, Lassmann, Waehneldt, Matthieu, & Linington, 1989). Enpp6 is required for the development of myelin sheath (Morita et al., 2016). Mobp plays a role in myelin compaction or stabilization (Montague, McCallion, Davies, & Griffiths, 2006). The Opalin is a myelin paranodal and inner loop protein (Yoshikawa et al., 2008). Sema6A regulates nodes of Ranvier in myelinating oligodendrocytes (Bernard et al., 2012). Spp1 is implicated in remyelination (Selvaraju et al., 2004). All these molecules are significantly downregulated in *Ulk4* mutants. Ulk4 therefore plays a major role in oligodendrogenesis and myelination.

However, the Ulk4 hypomyelination may also result from several aspects of indirect effects. First of all, Ulk4 is not a transcription factor but a member of the Ser/Thr kinase family. How Ulk4 regulates Olig2 expression is unknown, and at this stage there is no evidence that Ulk4 may bind Olig2 and/or post-translationally modify Olig2 and drive oligodendrogeneic lineage. Secondarily, oligodendroglial development and myelination can be regulated by axon-derived factors and neuroinflammation (Miron et al., 2011; Nave, 2010a,b; Nave & Werner, 2014). The axon inhibiting molecules *Cdh1*, *Vim* and *Gfap* (Menet, Prieto, Privat, & Gimenez y Ribotta, 2003; Ribotta, Menet, & Privat, 2004) are upregulated in *Ulk4*$^{tm1a/tm1a}$ mice, and we have shown evidence of smaller axon sizes in the mutant. Finally, the hydrocephalus phenotypes (Liu, Guan, Shen, Lalor, et al., 2016) and elevated neuroinflammation may affect the integrity of the white matter, which further contributes to the hypomyelination in the *Ulk4*$^{tm1a/tm1a}$ mice. *In vitro* cell culture experiments may be carried out in the future with commercial nanofibers of the same size, and this will demonstrate the contribution of small axons to the hypomyelination in *Ulk4* mutants (Lee, Chong, Tuck, Corey, & Chan, 2013; Lee et al., 2012). Targeted deletion of *Ulk4* gene in the oligodendroglial lineage, for example, by Cre-loxP genetic approach, may also provide an alternative approach.

While it is extremely important scientifically to work out the direct or indirect effects of the Ulk4 on myelination, the discovery of the strong hypomyelination phenotype in this report, together with other phenotype associated with ciliogenesis (Liu, Guan, Shen, Lalor, et al., 2016), neuritogenesis (Lang et al., 2014) and neurogenesis (Liu, Guan, Shen, Flinter, et al., 2016) in the *Ulk4* mutant mice, overwhelmingly highlight the importance of *ULK4* gene in human health. Haploinsufficiency in humans often presents severer phenotype than in heterozygous mice (Bi et al., 2002; Pandolfi et al., 1995; Van Esch & Devriendt, 2001; Zhang & Baldini, 2008). From clinical point of view, the understanding of the *Ulk4* hypomorph phenotype is therefore more meaningful to hemizygous deletions in patients (Lang et al., 2014; Liu, Guan, Shen, Flinter, et al., 2016). These phenotypes will provide a guidance role for the follow up studies of clinical imaging.

In summary, here we report a novel and important role of Ulk4 on myelination. The top dysregulated molecules in *Ulk4* hypomorph mutants are myelination-related and myelination is 50% reduced. ULK4 may become a novel drug target for diseases associated with white matter abnormality and hypomyelination.

ACKNOWLEDGMENT

Authors wish to acknowledge the staff of the Bio-Resources Unit, in particular Drs. Yolanda Garcia and Cathal O'Flatharta, for the support and assistance of experimental procedures; Pierce Lalor for the scientific and technical assistance at the Centre for Microscopy & Imaging, the facility funded by NUIG and the Irish Government's Programme for Research in Third Level Institutions, Cycles 4 and 5, National Development Plan 2007–2013. The authors acknowledge Dr Enda O'Connell for scientific and technical assistance and the facilities of the Genomics Core at the NUI Galway that is funded by NUIG and the Irish Government's Programme for Research in Third Level Institutions, Cycles 4 and 5, National Development Plan 2007–2013. Authors would also like to thank the KOMP Repository (www.KOMP.org), the Mouse Biology Program (www.mousebiology.org) at the UC Davis for supplying *Ulk4*$^{+/tm1a}$ breeding pairs.

CONFLICT OF INTEREST

The authors declare no conflict of interests.

ORCID

Una Fitzgerald http://orcid.org/0000-0002-8019-6546
Timothy O'Brien http://orcid.org/0000-0001-9028-5481
Sanbing Shen http://orcid.org/0000-0002-8217-9811

REFERENCES

Azim K, Butt AM. 2011. GSK3 beta negatively regulates oligodendrocyte differentiation and myelination in vivo. *Glia 59*:540–553. https://doi.org/10.1002/glia.21122

Azim K, Rivera A, Raineteau O, Butt AM. 2014. GSK3 beta regulates oligodendrogenesis in the dorsal microdomain of the subventricular zone via Wnt- beta- catenin signaling. *Glia 62*:778–789. https://doi.org/10.1002/glia.22641

Back SA, Rosenberg PA. 2014. Pathophysiology of glia in perinatal white matter injury. *Glia 62*:1790–1815. https://doi.org/10.1002/glia.22658

Baumann N, Pham-Dinh D. 2001. Biology of oligodendrocyte and myelin in the mammalian central nervous system. *Physiological Reviews 81*: 871–927.

Bernard F, Moreau-Fauvarque C, Heitz-Marchaland C, Zagar Y, Dumas L, Fouquet S, ... Chedotal A. 2012. Role of transmembrane semaphorin Sema6A in oligodendrocyte differentiation and myelination. *Glia 60*: 1590–1604. https://doi.org/10.1002/glia.22378

Bi W, Yan J, Stankiewicz P, Park SS, Walz K, Boerkoel CF, ... Lupski JR. 2002. Genes in a refined Smith-Magenis syndrome critical deletion interval on chromosome 17p11.2 and the syntenic region of the mouse. *Genome Research 12*:713–728. https://doi.org/10.1101/gr.73702

Brunner C, Lassmann H, Waehneldt TV, Matthieu JM, Linington C. 1989. Differential ultrastructural-localization of myelin basic-protein, myelin oligodendroglial glycoprotein, and 2',3'-cyclic nucleotide 3'-phosphodiesterase in the Cns of adult-rats. *Journal of Neurochemistry 52*:296–304. https://doi.org/DOI 10.1111/j.1471–4159.1989.tb10930.x

Bujalka H, Koenning M, Jackson S, Perreau VM, Pope B, Hay CM, ... Emery B. 2013. MYRF Is a membrane-associated transcription factor that autoproteolytically cleaves to directly activate myelin genes. *Plos Biology 11*:doi:ARTN e1001625-10.1371/journal.pbio.1001625

Caetano SC, Silveira CM, Kaur S, Nicoletti M, Hatch JP, Brambilla P, ... Soares JC. 2008. Abnormal corpus callosum myelination in pediatric bipolar patients. *Journal of Affective Disorders 108*:297–301. https://doi.org/10.1016/j.jad.2007.10.006

Cahoy JD, Emery B, Kaushal A, Foo LC, Zamanian JL, Christopherson KS, ... Barres BA. 2008. A transcriptome database for astrocytes, neurons, and oligodendrocytes: A new resource for understanding brain development and function. *Journal of Neuroscience 28*:264–278. https://doi.org/10.1523/Jneurosci.4178-07.2008

Chen Y, Miles DK, Hoang T, Shi J, Hurlock E, Kernie SG, Lu QR. 2008. The basic helix-loop-helix transcription factor Olig2 is critical for reactive astrocyte proliferation after cortical injury. *Journal of Neuroscience 28*:10983–10989. https://doi.org/10.1523/Jneurosci.3545-08.2008

Chen Y, Wu H, Wang SZ, Koito H, Li JR, Ye F, ... Lu QR. 2009. The oligodendrocyte-specific G protein-coupled receptor GPR17 is a cell-intrinsic timer of myelination. *Nature Neuroscience 12*:1398–1406. https://doi.org/10.1038/nn.2410

Chinnasamy D, Rudd R, Velakoulis D. 2006. A case of schizophrenia with complete agenesis of the corpus callosum. *Australas Psychiatry 14*:327–330. https://doi.org/10.1080/j.1440-1665.2006.02299.x

Demyanenko GP, Tsai AY, Maness PF. 1999. Abnormalities in neuronal process extension, hippocampal development, and the ventricular system of L1 knockout mice. *Journal of Neuroscience 19*:4907–4920.

Denninger AR, Breglio A, Maheras KJ, LeDuc G, Cristiglio V, Deme B, ... Kirschner DA. 2015. Claudin-11 tight junctions in myelin are a barrier to diffusion and lack strong adhesive properties. *Biophysical Journal 109*:1387–1397. https://doi.org/10.1016/j.bpj.2015.08.012

Emery B. 2010. Regulation of oligodendrocyte differentiation and myelination. *Science 330*:779–782. https://doi.org/10.1126/science.1190927

Fern R, Davis P, Waxman SG, Ransom BR. 1998. Axon conduction and survival in CNS white matter during energy deprivation: a developmental study. *Journal of Neurophysiology 79*:95–105.

Fields RD. 2008. White matter in learning, cognition and psychiatric disorders. *Trends in Neurosciences 31*:361–370. https://doi.org/10.1016/j.tins.2008.04.001

Franklin RJM, Gallo V. 2014. The translational biology of remyelination: Past, present, and future. *Glia 62*:1905–1915. https://doi.org/10.1002/glia.22622

From R, Eilam R, Bar-Lev DD, Levin-Zaidman S, Tsoory M, LoPresti P, ... Aharoni R. 2014. Oligodendrogenesis and myelinogenesis during postnatal development effect of glatiramer acetate. *Glia 62*:649–665. https://doi.org/10.1002/glia.22632

Giedd JN, Blumenthal J, Jeffries NO, Castellanos FX, Liu H, Zijdenbos A, ... Rapoport JL. 1999. Brain development during childhood and adolescence: a longitudinal MRI study. *Nature Neurosciences 2*:861–863. https://doi.org/10.1038/13158

Guo FZ, Lang J, Sohn J, Hammond E, Chang M, Pleasure D. 2015. Canonical Wnt Signaling in the Oligodendroglial Lineage-Puzzles Remain. *Glia 63*:1671–1693. https://doi.org/10.1002/glia.22813

Hatayama M, Ishiguro A, Iwayama Y, Takashima N, Sakoori K, Toyota T, ... Aruga J. 2011. Zic2 hypomorphic mutant mice as a schizophrenia model and ZIC2 mutations identified in schizophrenia patients. *Scientific Reports 1*:16-doi:10.1038/srep00016

Helman G, Van Haren K, Bonkowsky JL, Bernard G, Pizzino A, Braverman N, ... Consortium G. 2015. Disease specific therapies in leukodystrophies and leukoencephalopathies. *Molecular Genetics and Metabolism 114*:527–536. https://doi.org/10.1016/j.ymgme.2015.01.014

Hutchinson AD, Mathias JL, Jacobson BL, Ruzic L, Bond AN, Banich MT. 2009. Relationship between intelligence and the size and composition of the corpus callosum. *Experimental Brain Research 192*:455–464. https://doi.org/10.1007/s00221-008-1604-5

Hynd GW, Lorys AR, Semrudclikeman M, Nieves N, Huettner MIS, Lahey BB. 1991. Attention-deficit disorder without hyperactivity—A distinct

behavioral and neurocognitive syndrome. *Journal of Child Neurology 6*:S37–S43.

Innocenti GM, Ansermet F, Parnas J. 2003. Schizophrenia, neurodevelopment and corpus callosum. *Molecular Psychiatry 8*:261–274. https://doi.org/10.1038/sj.mp.4001205

Ishimoto T, Ninomiya K, Inoue R, Koike M, Uchiyama Y, Mori H. 2017. Mice lacking BCAS1, a novel myelin-associated protein, display hypomyelination, schizophrenia-like abnormal behaviors, and upregulation of inflammatory genes in the brain. *Glia 65*:727–739. https://doi.org/10.1002/glia.23129

Jungerius BJ, Hoogendoorn ML, Bakker SC, Van't Slot R, Bardoel AF, Ophoff RA, … Sinke RJ. 2008. An association screen of myelin-related genes implicates the chromosome 22q11 PIK4CA gene in schizophrenia. *Molecular Psychiatry 13*:1060–1068. https://doi.org/10.1038/sj.mp.4002080

Kettenmann H, Hanisch UK, Noda M, Verkhratsky A. 2011. Physiology of microglia. *Physiological Reviews 91*:461–553. https://doi.org/10.1152/physrev.00011.2010

Laclef C, Anselme I, Besse L, Catala M, Palmyre A, Baas D, … Schneider-Maunoury S. 2015. The role of primary cilia in corpus callosum formation is mediated by production of the Gli3 repressor. *Human Molecular Genetics 24*:4997–5014. https://doi.org/10.1093/hmg/ddv221

Lang B, Pu J, Hunter I, Liu M, Martin-Granados C, Reilly TJ, … Shen S. 2014. Recurrent deletions of ULK4 in schizophrenia: a gene crucial for neuritogenesis and neuronal motility. *Journal of Cell Sciences 127*:630–640. https://doi.org/10.1242/jcs.137604

Lang B, Song B, Davidson W, MacKenzie A, Smith N, McCaig CD, … Shen S. 2006. Expression of the human PAC1 receptor leads to dose-dependent hydrocephalus-related abnormalities in mice. *Journal of Clinical Investigation 116*:1924–1934. https://doi.org/10.1172/JCI27597

Larsen PH, DaSilva AG, Conant K, Yong VW. 2006. Myelin formation during development of the CNS is delayed in matrix metalloproteinase-9 and-12 null mice. *Journal of Neuroscience 26*:2207–2214. https://doi.org/10.1523/Jneurosci.1880-05.2006

Lee S, Chong SYC, Tuck SJ, Corey JM, & Chan JR. 2013. A rapid and reproducible assay for modeling myelination by oligodendrocytes using engineered nanofibers. *Nature Protocols 8*:771–782. https://doi.org/10.1038/nprot.2013.039

Lee S, Leach MK, Redmond SA, Chong SYC, Mellon SH, Tuck SJ, … Chan JR. 2012. A culture system to study oligodendrocyte myelination processes using engineered nanofibers. *Nature Methods 9*:917. https://doi.org/10.1038/nmeth.2105

Lehotzky A, Lau P, Tokeso N, Muja N, Hudson LD, Ovadv J. 2010. Tubulin Polymerization-Promoting Protein (TPPP/p25) is Critical for Oligodendrocyte Differentiation. *Glia 58*:157–168. https://doi.org/10.1002/glia.20909

Liu B, Chen X, Wang ZQ, Tong WM. 2014. Nbn Gene Inactivation in the CNS of Mouse Inhibits the Myelinating Ability of the Mature Cortical Oligodendrocytes. *Glia 62*:133–144. https://doi.org/10.1002/glia.22593

Liu M, Guan Z, Shen Q, Flinter F, Dominguez L, Ahn JW, … Shen S. 2016. Ulk4 regulates neural stem cell pool. *Stem Cells 34*:2318–2331. https://doi.org/10.1002/stem.2423

Liu M, Guan Z, Shen Q, Lalor P, Fitzgerald U, O'Brien T, … Shen S. 2016. Ulk4 is essential for ciliogenesis and CSF flow. *Journal of Neuroscience 36*:7589–7600. https://doi.org/10.1523/JNEUROSCI.0621-16.2016

Logan AM, Mammel AE, Robinson DC, Chin AL, Condon AF, Robinson FL. 2017. Schwann cell-specific deletion of the endosomal PI 3-kinase Vps34 leads to delayed radial sorting of axons, arrested myelination, and abnormal ErbB2-ErbB3 tyrosine kinase signaling. *Glia 65*:1452–1470. https://doi.org/10.1002/glia.23173

Lu QR, Sun T, Zhu Z, Ma N, Garcia M, Stiles CD, Rowitch DH. 2002. Common developmental requirement for Olig function indicates a motor neuron/oligodendrocyte connection. *Cell 109*:75–86.

Maggipinto MJ, Ford J, Le KH, Tutolo JW, Furusho M, Wizeman JW, … Barbarese E. 2017. Conditional Knockout of TOG Results in CNS Hypomyelination. *Glia 65*:489–501. https://doi.org/10.1002/glia.23106

Marcus J, Dupree JL, Popko B. 2002. Myelin-associated glycoprotein and myelin galactolipids stabilize developing axo-glial interactions. *Journal of Cell Biology 156*:567–577. https://doi.org/10.1083/jcb.200111047

Mathews ES, Mawdsley DJ, Walker M, Hines JH, Pozzoli M, Appel B. 2014. Mutation of 3-hydroxy-3-methylglutaryl CoA synthase I reveals requirements for isoprenoid and cholesterol synthesis in oligodendrocyte migration arrest, axon wrapping, and myelin gene expression. *Journal of Neuroscience 34*:3402–3412. https://doi.org/10.1523/JNEUROSCI.4587-13.2014

Mattan NS, Ghiani CA, Lloyd M, Matalon R, Bok D, Casaccia P, de Vellis J. 2010. Aspartoacylase deficiency affects early postnatal development of oligodendrocytes and myelination. *Neurobiology of Disease 40*:432–443. https://doi.org/10.1016/j.nbd.2010.07.003

Menet V, Prieto M, Privat A, Gimenez y, Ribotta M. 2003. Axonal plasticity and functional recovery after spinal cord injury in mice deficient in both glial fibrillary acidic protein and vimentin genes. *Proceedings of the National Academy of Sciences of the United States of America 100*:8999–9004. https://doi.org/10.1073/pnas.1533187100

Miron VE, Kuhlmann T, Antel JP. 2011. Cells of the oligodendroglial lineage, myelination, and remyelination. *Biochimica et Biophysica Acta 1812*:184–193. https://doi.org/10.1016/j.bbadis.2010.09.010

Montague P, McCallion AS, Davies RW, Griffiths IR. 2006. Myelin-associated oligodendrocytic basic protein: A family of abundant CNS myelin proteins in search of a function. *Developmental Neuroscience 28*:479–487. https://doi.org/10.1159/000095110

Morita J, Kano K, Kato K, Takita H, Sakagami H, Yamamoto Y, … Aoki J. 2016. Structure and biological function of ENPP6, a choline-specific glycerophosphodiester-phosphodiesterase. *Scientific Reports 6*:doi: ARTN 2099510.1038/srep20995

Motomura N, Satani S, Inaba M. 2002. Monozygotic twin cases of the agenesis of the corpus callosum with schizophrenic disorder. *Psychiatry and Clinical Neurosciences 56*:199–202. https://doi.org/DOI 10.1046/j.1440–1819.2002.00944.x

Nave KA. 2010a. Myelination and support of axonal integrity by glia. *Nature 468*:244–252. https://doi.org/10.1038/nature09614

Nave KA. 2010b. Myelination and the trophic support of long axons. *Nature Reviews Neuroscience 11*:275–283. https://doi.org/10.1038/nrn2797

Nave KA, Werner HB. 2014. Myelination of the nervous system: mechanisms and functions. *Annual Review of Cell and Developmental Biology 30*:503–533. https://doi.org/10.1146/annurev-cellbio-100913-013101

Nicolay DJ, Doucette JR, Nazarali AJ. 2007. Transcriptional control of oligodendrogenesis. *Glia 55*:1287–1299. https://doi.org/10.1002/glia.20540

Pandolfi PP, Roth ME, Karis A, Leonard MW, Dzierzak E, Grosveld FG, … Lindenbaum MH. 1995. Targeted disruption of the GATA3 gene causes severe abnormalities in the nervous system and in fetal liver haematopoiesis. *Nature Genetics 11*:40–44. https://doi.org/10.1038/ng0995-40

Paul LK, Brown WS, Adolphs R, Tyszka JM, Richards LJ, Mukherjee P, Sherr EH. 2007. Agenesis of the corpus callosum: genetic, developmental and functional aspects of connectivity. *Nature Reviews Neuroscience 8*:287–299. https://doi.org/10.1038/nrn2107

Penke L, Maniega SM, Murray C, Gow AJ, Hernandez MCV, Clayden JD, … Deary IJ. 2010. A general factor of brain white matter integrity predicts

information processing speed in healthy older people. *Journal of Neuroscience 30*:7569–7574. https://doi.org/10.1523/Jneurosci.1553-10.2010

Potter KA, Kern MJ, Fullbright G, Bielawski J, Scherer SS, Yum SW, ... Hama H. 2011. Central nervous system dysfunction in a mouse model of FA2H deficiency. *Glia 59*:1009–1021. https://doi.org/10.1002/glia.21172

Pujol J, Lopez-Sala A, Sebastian-Galles N, Deus J, Cardoner N, Soriano-Mas C, ... Sans A. 2004. Delayed myelination in children with developmental delay detected by volumetric MRI. *Neuroimage 22*:897–903. https://doi.org/10.1016/j.neuroimage.2004.01.029

Ribotta MG, Menet V, Privat A. 2004. Glial scar and axonal regeneration in the CNS: lessons from GFAP and vimentin transgenic mice. *Acta Neurochirurgica (Suppl) 89*:87–92.

Schaerenwiemers N, Schaefer C, Valenzuela DM, Yancopoulos GD, Schwab ME. 1995. Identification of new oligodendrocyte-specific and myelin-specific genes by a differential screening approach. *Journal of Neurochemistry 65*:10–22.

Schiffmann R, van der Knaap MS. 2009. Invited article: an MRI-based approach to the diagnosis of white matter disorders. *Neurology 72*:750–759. https://doi.org/10.1212/01.wnl.0000343049.00540.c8

Selvaraju R, Bernasconi L, Losberger C, Graber P, Kadi L, Avellana-Adalid V, ... Boschert U. 2004. Osteopontin is upregulated during in vivo demyelination and remyelination and enhances myelin formation in vitro. *Molecular and Cellular Neuroscience 25*:707–721. https://doi.org/10.1016/j.mcn.2003.12.014

Sforazzini F, Bertero A, Dodero L, David G, Galbusera A, Scattoni ML, ... Gozzi A. 2016. Altered functional connectivity networks in acallosal and socially impaired BTBR mice. *Brain Structure and Functions 221*:941–954. https://doi.org/10.1007/s00429-014-0948-9

Shen S, Lang B, Nakamoto C, Zhang F, Pu J, Kuan SL, ... St Clair D. 2008. Schizophrenia-related neural and behavioral phenotypes in transgenic mice expressing truncated Disc1. *Journal of Neuroscience 28*:10893–10904. https://doi.org/10.1523/JNEUROSCI.3299-08.2008

Skarnes WC, Rosen B, West AP, Koutsourakis M, Bushell W, Iyer V, ... Bradley A. 2011. A conditional knockout resource for the genome-wide study of mouse gene function. *Nature 474*:337–342. https://doi.org/10.1038/nature10163

Steenweg ME, Vanderver A, Blaser S, Bizzi A, de Koning TJ, Mancini GM, ... van der Knaap MS. 2010. Magnetic resonance imaging pattern recognition in hypomyelinating disorders. *Brain 133*:2971–2982. https://doi.org/10.1093/brain/awq257

Sun F, Lin CLG, Mctigue D, Shan X, Tovar CA, Bresnahan JC, & Beattie MS. 2010. Effects of Axon Degeneration on Oligodendrocyte Lineage Cells: Dorsal Rhizotomy Evokes a Repair Response While Axon Degeneration Rostral to Spinal Contusion Induces Both Repair and Apoptosis. *Glia 58*:1304–1319. https://doi.org/10.1002/glia.21009

Swayze VW, Johnson VP, Hanson JW, Piven J, Sato Y, Giedd JN, ... Andreasen NC. 1997. Magnetic resonance imaging of brain anomalies in fetal alcohol syndrome. *Pediatrics 99*:232–240. https://doi.org/DOI 10.1542/peds.99.2.232

Takei F, Shapiro K, Hirano A, Kohn I. 1987. Influence of the rate of ventricular enlargement on the ultrastructural morphology of the white matter in experimental hydrocephalus. *Neurosurgery 21*:645–650.

Thakurela S, Garding A, Jung RB, Muller C, Goebbels S, White R, ... Tiwari VK. 2016. The transcriptome of mouse central nervous system myelin. *Scientific Reports 6*:25828-doi:10.1038/srep25828

van Eimeren L, Niogi SN, McCandliss BD, Holloway ID, Ansari D. 2008. White matter microstructures underlying mathematical abilities in children. *Neuroreport 19*:1117–1121. https://doi.org/10.1097/WNR.0b013e328307f5c1

Van Esch H, Devriendt K. 2001. Transcription factor GATA3 and the human HDR syndrome. *Cellular and Molecular Life Sciences 58*:1296–1300.

Wolf RC, Hose A, Frasch K, Walter H, Vasic N. 2008. Volumetric abnormalities associated with cognitive deficits in patients with schizophrenia. *European Psychiatry 23*:541–548. https://doi.org/10.1016/j.eurpsy.2008.02.002

Wolff JJ, Gerig G, Lewis JD, Soda T, Styner MA, Vachet C, ... Network I. 2015. Altered corpus callosum morphology associated with autism over the first 2 years of life. *Brain 138*:2046–2058. https://doi.org/10.1093/brain/awv118

Xie D, Shen FC, He SR, Chen MM, Han QP, Fang M, ... Deng YY. 2016. IL-1 beta induces hypomyelination in the periventricular white matter through inhibition of oligodendrocyte progenitor cell maturation via FYN/MEK/ERK signaling pathway in septic neonatal rats. *Glia 64*:583–602. https://doi.org/10.1002/glia.22950

Yoshikawa F, Sato Y, Tohyama K, Akagi T, Hashikawa T, Nagakura-Takagi Y, ... Furuichi T. 2008. Opalin, a transmembrane sialylglycoprotein located in the central nervous system myelin paranodal loop membrane. *Journal of Biological Chemistry 283*:20830–20840. https://doi.org/10.1074/jbc.M801314200

Yuelling LW, Waggener CT, Afshari FS, Lister JA, Fuss B. 2012. Autotaxin/ENPP2 regulates oligodendrocyte differentiation in vivo in the developing zebrafish hindbrain. *Glia 60*:1605–1618. https://doi.org/10.1002/glia.22381

Zhang Y, Chen K, Sloan SA, Bennett ML, Scholze AR, O'Keeffe S, ... Wu JQ. 2014. An RNA-sequencing transcriptome and splicing database of glia, neurons, and vascular cells of the cerebral cortex. *Journal of Neuroscience 34*:11929–11947. https://doi.org/10.1523/JNEUROSCI.1860-14.2014

Zhang Z, Baldini A. 2008. In vivo response to high-resolution variation of Tbx1 mRNA dosage. *Human Molecular Genetics 17*:150–157. https://doi.org/10.1093/hmg/ddm291

Zhao LX, Ku L, Chen Y, Xia M, LoPresti P, Feng Y. 2006. QKI binds MAP1B mRNA and enhances MAP1B expression during oligodendrocyte development. *Molecular Biology of the Cell 17*:4179–4186. https://doi.org/10.1091/mbc.E06-04-0355

Zhou J, Wen YQ, She L, Sui YN, Liu L, Richards LJ, Poo MM. 2013. Axon position within the corpus callosum determines contralateral cortical projection. *Proceedings of the National Academy of Sciences of the United States of America 110*:E2714–E2723. https://doi.org/10.1073/pnas.1310233110

Zhou Q, Choi G, Anderson DJ. 2001. The bHLH transcription factor Olig2 promotes oligodendrocyte differentiation in collaboration with Nkx2.2. *Neuron 31*:791–807.

Zhu H, Zhao L, Wang E, Dimova N, Liu G, Feng Y, Cambi F. 2012. The QKI-PLP pathway controls SIRT2 abundance in CNS myelin. *Glia 60*:69–82. https://doi.org/10.1002/glia.21248

SUPPORTING INFORMATION

Additional Supporting Information may be found online in the supporting information tab for this article.

How to cite this article: Liu M, Xu P, Guan Z, et al. *Ulk4* deficiency leads to hypomyelination in mice. *Glia*. 2018;66:175–190. https://doi.org/10.1002/glia.23236